Analysis and Testing of a Highly Skewed Bridge

by

MICHAEL J. CHAJES
HARRY W. SHENTON III
HAOXIONG HUANG

Department of Civil & Environmental Engineering
University of Delaware
Newark, Delaware 19716

DELAWARE TRANSPORTATION INSTITUTE
University of Delaware
Newark, Delaware 19716

This work was sponsored by the Delaware Transportation Institute and was prepared in cooperation with the Delaware Department of Transportation. The contents of this report reflect the views of the authors who are responsible for the facts and accuracy of the data presented herein. The contents do not necessarily reflect the official views of the Delaware Transportation Institute or the Delaware Department of Transportation at the time of publication. This report does not constitute a standard, specification, or regulation.

Analysis and Testing of a Highly Skewed Bridge

Executive Summary

This report summarizes the results of an investigation of the behavior of a recently constructed, highly skewed, slab-on-steel girder bridge. A program of field testing and numerical modeling was undertaken to study the behavior of the bridge and to compare the results obtained by using the AASHTO LRFD formulas for load distribution to the field test and model results.

The bridge studied in this investigation is denoted as 2-914 in the state bridge inventory. It carries SR1 over Route 13 in Kent county Delaware. The bridge consists of two identical, parallel structures for the southbound and northbound roadways, respectively, each having two lanes and two shoulders. Each bridge is a two span, continuous, slab-on-steel girder, composite superstructure with a skew of 60 degrees. The bridge was designed according to the 1989 AASHTO Standard Specifications for Highway Bridges, using the load factor design method. Construction of the bridge was completed in 1995.

A diagnostic load test was conducted of the bridge on June 11, 1997. The test focused on the west span of the northbound bridge. Forty strain transducers were mounted to various locations on the steel girders: four to top flange locations and thirty-six to bottom flange locations. Transducers were layed out along lines normal to the girder axes and parallel to the abutment (skew direction). Two fully loaded dump trucks were used as the load for the test. The gross vehicle weights were 60.95 kips and 57.5 kips, respectively. The trucks made a total of 13 passes across the bridge along various transverse positions. This included 9 single vehicle passes and 4 dual vehicle passes. Strains were continuously recorded as the vehicles crossed the bridge at a crawl speed (5 mph)

For the single truck passes, the absolute maximum strain recorded was 72 με and the maximum negative strain was 38 με. These correspond to live load stresses of 2.2 ksi and 1.1 ksi, respectively. For the dual truck passes the absolute maxmimum strain recorded was 94 με and the maximum negative strain was 48 με. These correspond to live load stresses of 2.8 ksi in tension and 1.4 ksi in compression. Contour plots of strain in the girders were generated from the measured data and show that the strain (load) distributes more or less parallel to the skew line, and is fairly narrow, i.e., is concentrated in the girder directly under the load. Although the girders are "pinned," negative bending was observed near the support in the obtuse corner. This may be due to the cross frame diaphragms and the bridge skew. Superposition of the single truck pass results compared favourably with the dual truck pass results, indicating that the bridge is in fact behaving linearly.

A three-dimensional finite element model of the bridge was developed using the commercial program ANSYS. The reinforced concrete deck was modeled using elastic shell elements, the steel girders were modeled using elastic beam elements, as were the diaphragm cross frames.

Composite action between the deck and girders was modeled using rigid connections and constraint equations. The influence of several modeling details was investigated, including mesh size, diaphragm stiffness, Young's modulus of the concrete and details of the bearing support. The loading on the model corresponded to the dual truck pass 11, with the trucks in the position that caused the largest measured strain in the test.

A convergence study showed that the model mesh size was sufficiently small to yield converged results. Parametric studies also showed that a +/-10% variation in the Young's modulus of the concrete had little influence on the computed transverse load distribution in the bridge. A more detailed model of the bridge bearings also had little influence on the transverse load distribution in the bridge, when compared to the simple pin support model. The stiffness of the diaphragm cross frames, however, had a significant affect on the load distribution in the bridge. With diaphragms present the absolute maximum computed strain decreased and there was greater transverse load distribution, relative to the results obtained without diaphragms. The diaphragms were found to have an effect on the strains near the supports; negative bending was observed near the supports closest to the load when the diaphragms were present, which is consistent with the experimental results.

The finite element results were compared to the measured data for all thirteen truck passes. Overall the analytical model was stiffer than the real structure, although the results were generally consistent with the measurements. The differences between the measured and computed peak strains varied from a low of 1% to a high of 27%. The calculated values were consistently smaller than the measured values, which again indicates that the model is stiffer than the actual bridge. One possible explaination for the model being stiffer is that in the negative moment region the concrete is in tension, which would yield a lower effective stiffness of the composite section than used in the model.

The recently published AASHTO LRFD Standard Specification for Highway Bridges includes new equations for transverse load distribution that are a function of, among other parameters, skew. A comparison was made between the load distribution factors predicted by the new AASHTO formulas and the test results. For positive moment, the measured load distribution factors for a single lane loaded and two lanes loaded were significantly smaller than those given by the AASHTO formulas, in some cases by as much as a factor of 2. For negative moment, the measured load distribution factors for a single lane loaded and two lanes loaded were very close to the factors predicted by the AASHTO formulas. The results indicate that the AASHTO formulas appear to be conservative for positive moment and accurate for negative moment.

Three key conclusions and recommendation can be drawn from this investigation:

2. The recently published AASHTO LRFD formulas for transverse load distribution appear to be conservative for positive bending (based on detailed testing and analysis of this one bridge), for concrete-on-steel girder bridges with skews as large as 60 degrees and can be used with confidence.

3. The recently published AASHTO LRFD formulas for transverse load distribution appear to be accurate but not conservative for negative bending (based on detailed testing and analysis of this one bridge), for concrete-on-steel girder bridges with skews as large as 60 degrees and should be applied in design with this in mind.

3. Full scale field testing, in conjunction with three dimensional finite element modeling proved to be very informative in understanding and predicting the behavior of this type of structure. These techniques may be applied with confidence in the future to other unique or problematic structures.

TABLE OF CONTENTS

LIST OF TABLES

LIST OF FIGURES

ABSTRACT

Continuous composite slab-on-girder bridges remain one of the most common types built. If possible, bridges are constructed such that their span direction is perpendicular to the bridge abutments. This type of bridge is called a "right" bridge. Highly skewed bridges can be the result of various design constraints. The proper design of all new bridges and evaluation of existing ones require accurate prediction of their behavior. The American Association of State Highway and Transportation Official (AASHTO) specifications provide a simple live load distribution factor method for designing bridges. In order to get accurate load distribution factors, one must understand the behavior of the bridge. While the behavior of right bridges and bridges with limited skews are relatively well understood, the behavior of highly skewed bridges is not. In order to better understand the behavior, this research introduces a field test and numerical analyses of a highly skewed bridge. The bridge tested and analyzed is a two span, continuous, slab-on-girder composite highway bridge with a skew angle of 60°. The behavior of the skewed bridge is defined based on the field test data. Finite element analyses of the bridge were conducted using ANSYS to investigate the influence of model mesh, transverse stiffness, diaphragms, and modeling of the supports. The resulting test and analytical results were then compared with AASHTO's suggested formulas for live load distribution.

Chapter 1

INTRODUCTION

1.1 Motivation

Bridges play an important role in the highway system and infrastructure of society. The cost to society of a poorly designed, constructed or maintained bridge can be tremendous. Accurate knowledge of the load-carrying capacity and load distribution in a bridge are paramount to insure satisfactory performance of the bridge.

Although modern computer techniques can provide detailed information about the load distribution in a bridge, the American Association of State Highway and Transportation Official (AASHTO) bridge design specifications [1] provide a simple method for determining live load distribution, such that the bridge can be designed and analyzed as a series of beams, rather than a more complex three dimensional structure. This makes routine design easy and provides a simple and quick way to evaluate a bridge. The AASHTO approach, however, depends on having accurate live load distribution factors for all types and configurations of bridges.

A skewed bridge is one whose longitudinal axis forms an acute angle with the abutment. The configuration of such a structure can be the result of many things including natural or man-made obstacles, complex intersections, space limitations, or mountainous terrain. Some investigations have been conducted on the influence of skew on load distribution. Most works, however, were based on model tests and finite

element analyses. Few full-scale field tests have been conducted to verify the AASHTO live load distribution factor for highly skewed bridges.

1.2 AASHTO Load Distribution Factors

The AASHTO LRFD Bridge Design Specifications [1] provides a detailed and simple live load distribution factor method for normal bridge design. Until recently, the load distribution factor was simply determined by the expression *s*/7, in which *s* is the girder spacing; no effect of skew was considered. In the amendments of 1996 and 1997 to the 1994 edition, the effects of beam spacing, span, longitudinal stiffness, and depth of slab were included. The effect of skew was considered as a reduction factor applied to the normal load distribution factor. The load distribution formulas for a concrete deck on steel girder bridge, per the AASHTO specification are as follows.

The distribution factor for moment in an interior beam is

$$g = 0.06 + \left(\frac{S}{4300}\right)^{0.4}\left(\frac{S}{L}\right)^{0.3}\left(\frac{K_g}{Lt_s^3}\right)^{0.1} \tag{1.1}$$

in the case of one design lane loaded or

$$g = 0.075 + \left(\frac{S}{2900}\right)^{0.6}\left(\frac{S}{L}\right)^{0.2}\left(\frac{K_g}{Lt_s^3}\right)^{0.1} \tag{1.2}$$

in the case of two or more design lanes loaded, in which,

g = load distribution factor;

S = spacing of beams (mm);

L = span of beam (mm);

$K_g = n\left(I + Ae_g^2\right)$: longitudinal stiffness parameter (mm^4);

$n = \frac{E_B}{E_D}$: modulus ratio;

E_B = modulus of elasticity of beam material (MPa);

E_D = modulus of elasticity of deck material (MPa);

I = moment of inertia of beam (mm^4);

A = sectional area of beam (mm^2);

e_g = distance between the centers of gravity of the basic beam and deck (mm);

t_s = depth of concrete slab (mm);

The distribution factor for moment in an exterior beam can be determined by the Lever Rule in the case of one design lane loaded, or by applying an adjustment coefficient to the factor for an interior beam, $g_{exterior} = eg_{interior}$, where

$$e = 0.77 + \frac{d_e}{2800} \tag{1.3}$$

and d_e is the distance from the web of the exterior beam to the interior edge of the curb or traffic barrier in millimeters.

The effect of the skew is considered as a reduction factor,

$$c = 1 - c_1(\tan\theta)^{1.5} \tag{1.4}$$

applied to the above factors, where $c_1 = 0.25\left(\frac{K_g}{Lt_s^3}\right)^{0.25}\left(\frac{S}{L}\right)^{0.5}$ and θ is the skew angle in degree.

1.3 Previous Work

Khaled and Itani (1990) used the finite element method to determine moments in continuous normal and skew slab-and-girder bridges due to live loads. Their analyses showed that the maximum moment in the girder of a skewed bridge

was smaller than that of a normal bridge; approximately 20% less for a bridge with a skew angle of 60°.

Zokaie, et al. (1991) developed load distribution factor formulas and adjustments for various types of bridges, e.g., slab on girder, box girder, slab, multi-box beam, and spread box beam bridges. Three levels of analysis were performed on an "average bridge," a hypothetical bridge that has all the average properties obtained from the database of a few hundred actual bridges selected randomly from various states. The effects of girder spacing, span length, longitudinal stiffness, and slab thickness were included. The effect of skew was considered as a reduction factor applied to the normal load distribution factor. This research was the basis for the AASHTO formulas.

Ebeido and Kennedy (1995 and 1996) tested three model bridges, one with a skew angle of 0° and two with skew angles of 45°, supported at the two ends and continuous over the intermediate pier support. A parametric study using the finite element method was conducted to investigate the influence of all major parameters affecting moment, shear and reaction distribution factors in the elastic range of loading. Empirical formulas for the distribution factors were developed. These factors were slightly different from that defined by the AASHTO Specifications (1994).

Mabsout, et al. (1997) compared four finite element modeling methods to determine load distribution factors for a one-span, two-lane, simply supported, composite steel girder bridge. In the first method the concrete slab was modeled with quadrilateral shell elements and the steel girders were idealized as space frame members. The centroid of each girder coincided with the centroid of concrete slab. In

the second method the concrete slab was modeled with quadrilateral shell elements and eccentrically connected space frame members representing the girders. In the third method the concrete slab and steel girder web were modeled with quadrilateral shell elements, girder flanges were modeled as space frame elements, while flange to deck eccentricity was modeled by imposing a rigid link. In the fourth method, the concrete slab was modeled with isotropic eight node brick elements; the steel girder flanges and webs were modeled with quadrilateral shell elements. The four finite element models produced similar load distribution factors. The results indicated that the concrete slab could be modeled with sufficient accuracy as quadrilateral shell elements and the girders as space frame elements.

1.4 Scope and Objectives

This research focused on the behavior of a highly skewed slab-on-girder bridge. A slab-on-girder bridge with a skew angle of 60° located in Delaware was field tested. Theoretical analyses using the finite element method were conducted. The results of the theoretical analysis were compared with the test results and the AASHTO specifications for load distribution.

The main objective of the project was to experimentally evaluate the load distribution for the highly skewed bridge and compare the measured load distribution factors to analytical predictions and predictions resulting from the AASHTO formulas. Information on field test results and finite element analyses are presented.

1.5 Outline of Report

Chapter 1 presents a general introduction to the project, including motivation, scope and objectives. A review of previous work is also included in this

chapter. Chapter 2 introduces the bridge that was tested. Chapter 3 explains the test, including test setup and test procedures. Test results are also presented in Chapter 3. Chapter 4 presents the finite element analyses that were conducted, including modeling of the bridge and analysis results. Conclusions are given in Chapter 5.

Chapter 2

BRIDGE DESCRIPTION

The bridge that was tested and analyzed in this investigation carries Route 1 traffic over Route 13 in Kent County, Delaware. The structure is identified as bridge 1-914 in the state inventory. It consists of two parallel, identical bridges for the southbound and northbound roadways, respectively, each having two lanes and two shoulders. Each bridge has a two span, continuous, slab-on-steel-girder, composite superstructure with a skew of 60°. The bridge was designed according to the 1989 AASHTO Standard Specifications for Highway Bridges, using the load factor design method.

A plan view of the bridge is shown in Figure 2.1. The bridge consists of two equal spans of 165 feet each. There are six steel plate girders spaced at a distance of 9 feet; a typical girder elevation is shown in Figure 2.2. The section properties of the girders vary along the span; four different sections are used.

A section view of the bridge is shown in Figure 2.3. The deck consists of a nine-inch thick cast in place concrete slab. The composite slab and girders are connected by shear studs spaced at a distance of 11 inches or 24 inches, as shown in Figure 2.4. The girders are connected by transverse diaphragms, spaced approximately every 20.5 feet, which are perpendicular to the girders. Details of the diaphragms are shown in Figure 2.5. Specifications for the bridge call for a steel strength of 50,000 psi and a slab concrete strength of 4,500 psi.

The bridge is simply supported at each end on expansion bearings and is continuous over the center pier, where it is supported by a fixed bearing. Details of the bearings are shown in Figures 2.6 and 2.7.

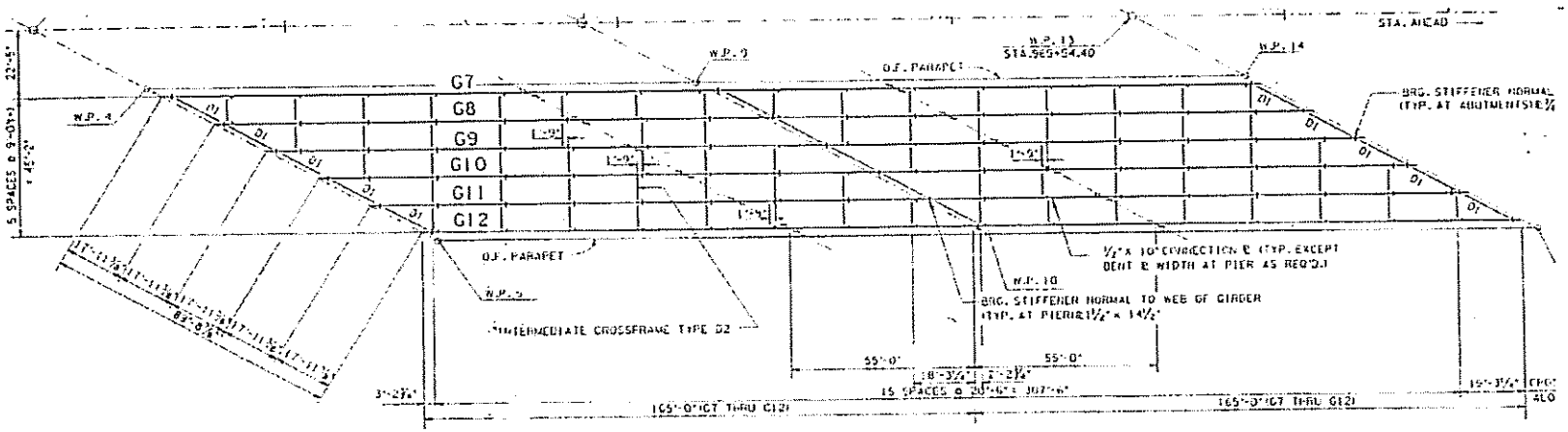

Figure 2.1 Plan view of the bridge

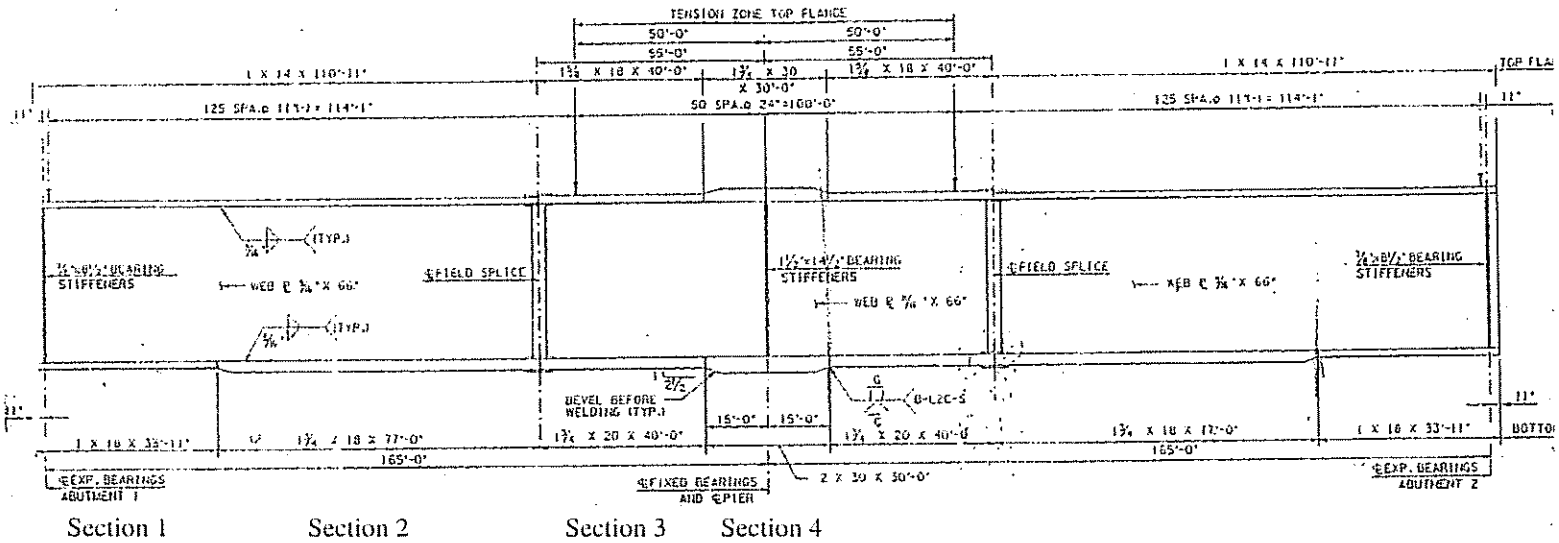

Figure 2.2 Girder elevation

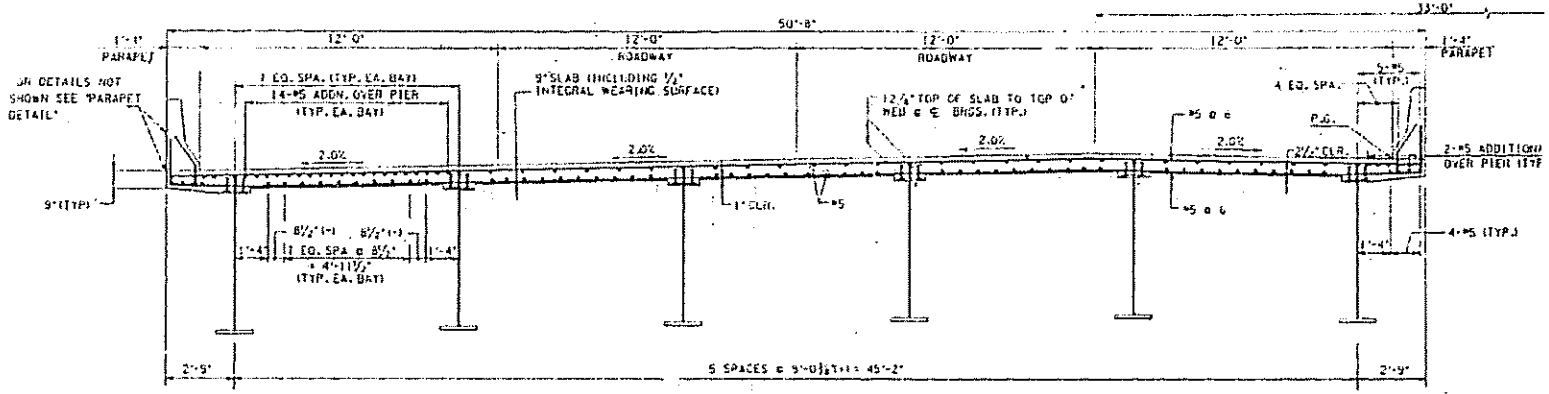

Figure 2.3 Section view of the bridge

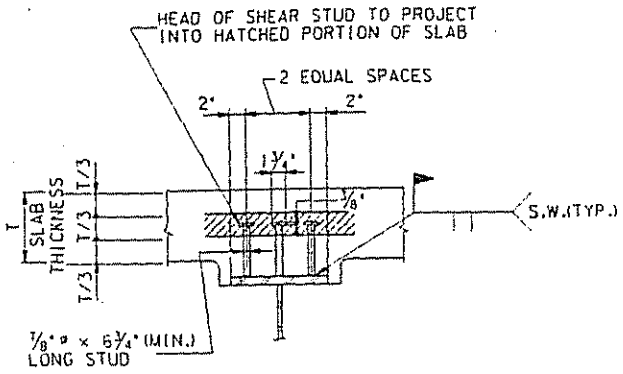

Figure 2.4 Shear stud connecting slab and girders

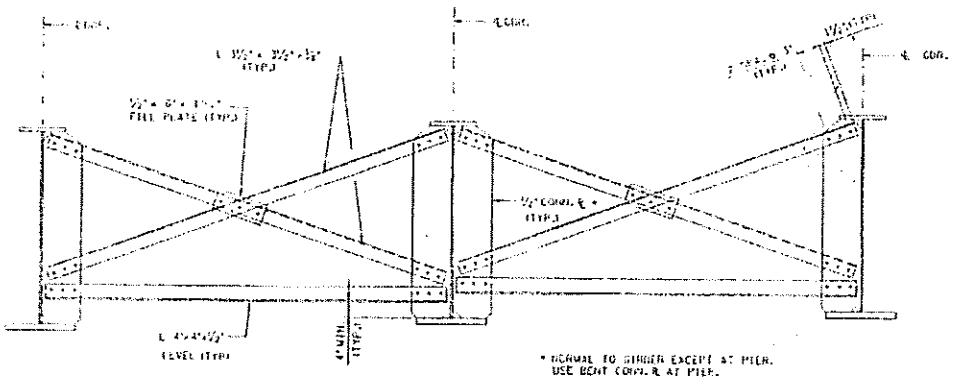

a. Intermediate cross-frame

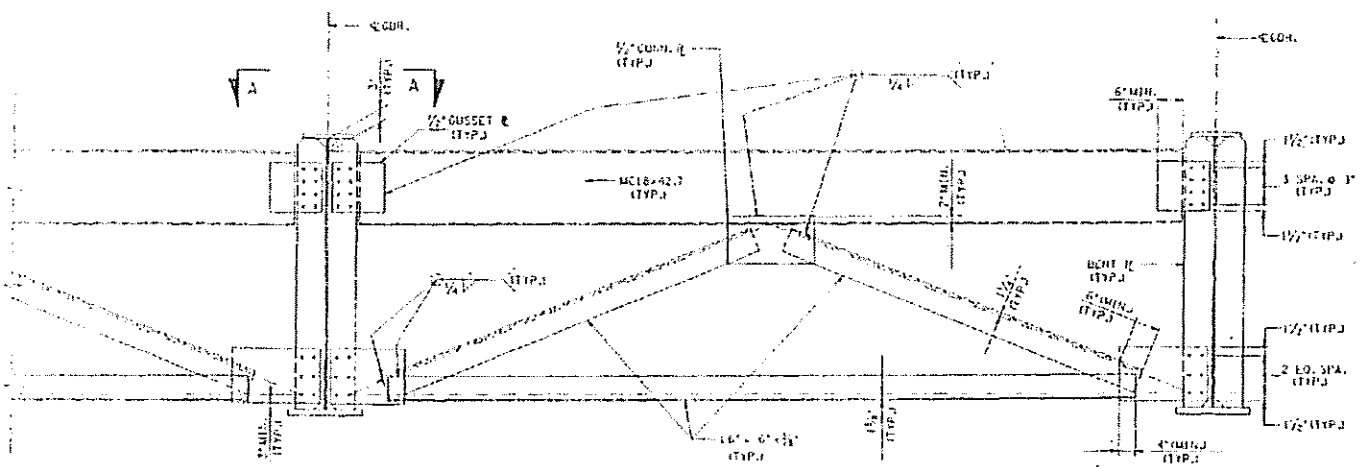

b. End cross-frame

Figure 2.5 Diaphragms

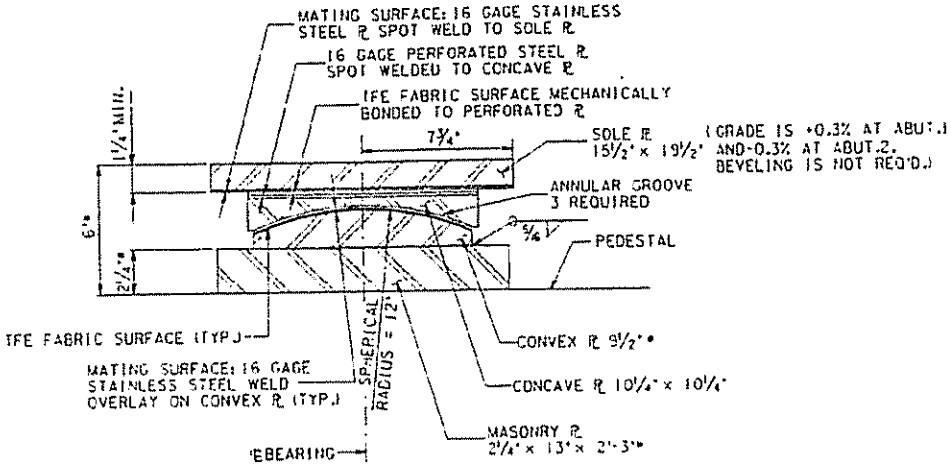

Figure 2.6 Expansion bearing

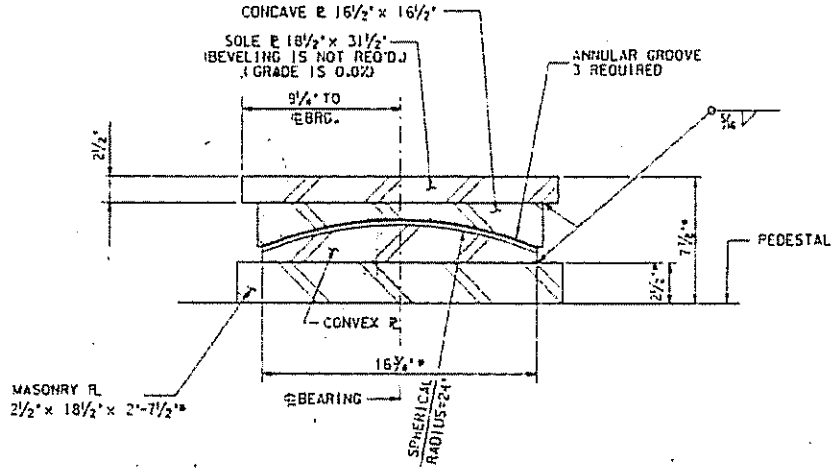

Figure 2.7 Fixed bearing

Chapter 3

FIELD TEST OF BRIDGE

3.1 Overview

A full-scale field test of the bridge was conducted on June 11, 1997. Preweighed trucks were used to load the bridge. The trucks crossed the bridge along several different load paths and the bridge response was measured. The measured response included strains in the top and bottom flange of several girders at several different locations.

Conditions were clear and sunny in the morning and cloudy in the afternoon on the test date. The temperature was approximately 80°F. The test lasted 8 hours, including setup and take-down of the instrumentation.

An instrumentation and data acquisition system, developed specifically for field testing of bridges by Bridge Diagnostics, Incorporated (BDI), was used. Forty BDI strain transducers were used, four on the top flanges and thirty-six on the bottom flanges of the steel girders.

The bridge was tested under carefully controlled load conditions. Two fully loaded dump trucks were used as the loads for the test. The trucks crossed the bridge along designated longitudinal lines at a speed of between 3 to 5 miles per hour. Thirteen truck passes were made.

3.2 Test Set-up

3.2.1 Test System

The test was conducted using Bridge Diagnostics Incorporated (BDI) Structural Testing System. The system consists of five main components: laptop computer, power supply/interface unit, four-channel data acquisition modules, strain transducers, and cables. The system, as currently configured, includes ten four-channel data acquisition modules, forty strain transducers and over five hundred feet of interconnecting cable. Each strain transducers comes with twenty feet of integral cable. A radio transmitter is used to record the position of the truck on the bridge, as described later. A schematic diagram of the test system is shown in Figure 3.2.1.

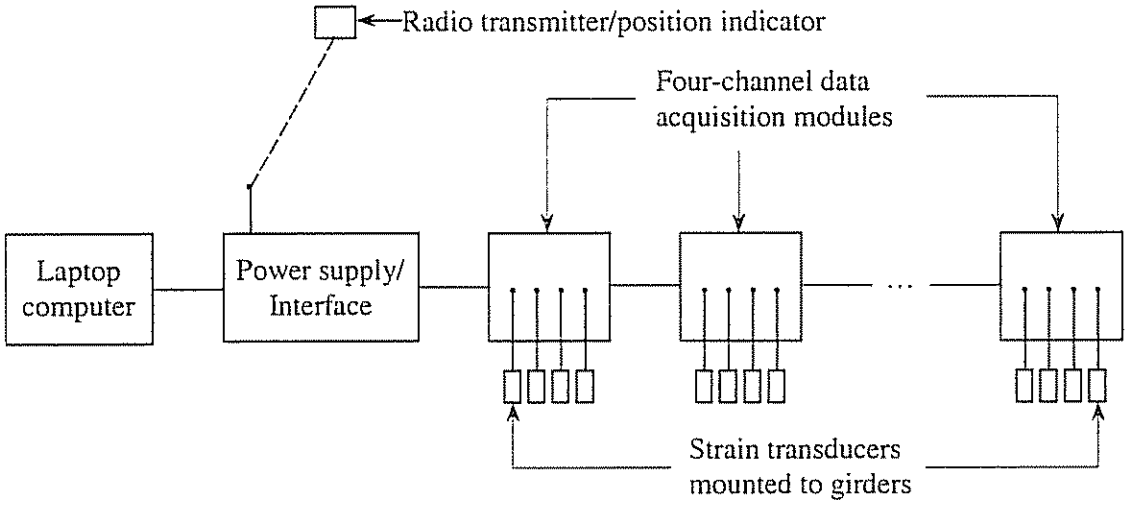

Figure 3.2.1 Test system

3.2.2 Instrumentation and Data Acquisition

The transducers used to measure strain were BDI "Intelliducers", which consist of four foil strain gages in a modified Wheatstone bridge configuration mounted to a steel ring. The transducer measures axial strain along its principal axis and can be easily attached to a member using either c-clamps or bonded stud mounts. Each "Intelliducer" contains a small microchip that gives the device a unique identity. When the transducer is connected to the data acquisition system it is automatically identified by the system; therefore, there is no need to manually note which transducer is connected to which channel. This is very beneficial when conducting large-scale field tests. The transducers are identified by a three-digit number. The transducer can be mounted and removed quickly and easily and can be used repeatedly.

Data acquisition takes place at the four-channel data acquisition modules. The digital data is then relayed back to the laptop computer via the parallel interface. This arrangement eliminates the problem of noise which is typically a concern with cable runs of fifty feet or more.

3.2.3 Transducer Layout

Only one span of the two span continuous bridge was instrumented. Measurements were focused on the west span of the northbound bridge, as shown in Figure 3.2.2. Forty BDI transducers were deployed to various locations on the steel girders, as shown in Figure 3.2.3. Four transducers were mounted to the top flanges of girders and thirty-six were mounted to the bottom flange. The transducers on the bottom flanges were mounted using c-clamps. The transducers on the top flanges were mounted using bonded stud mounts. A sketch showing the gages mounted to the top and bottom flanges is presented in Figure 3.2.4.

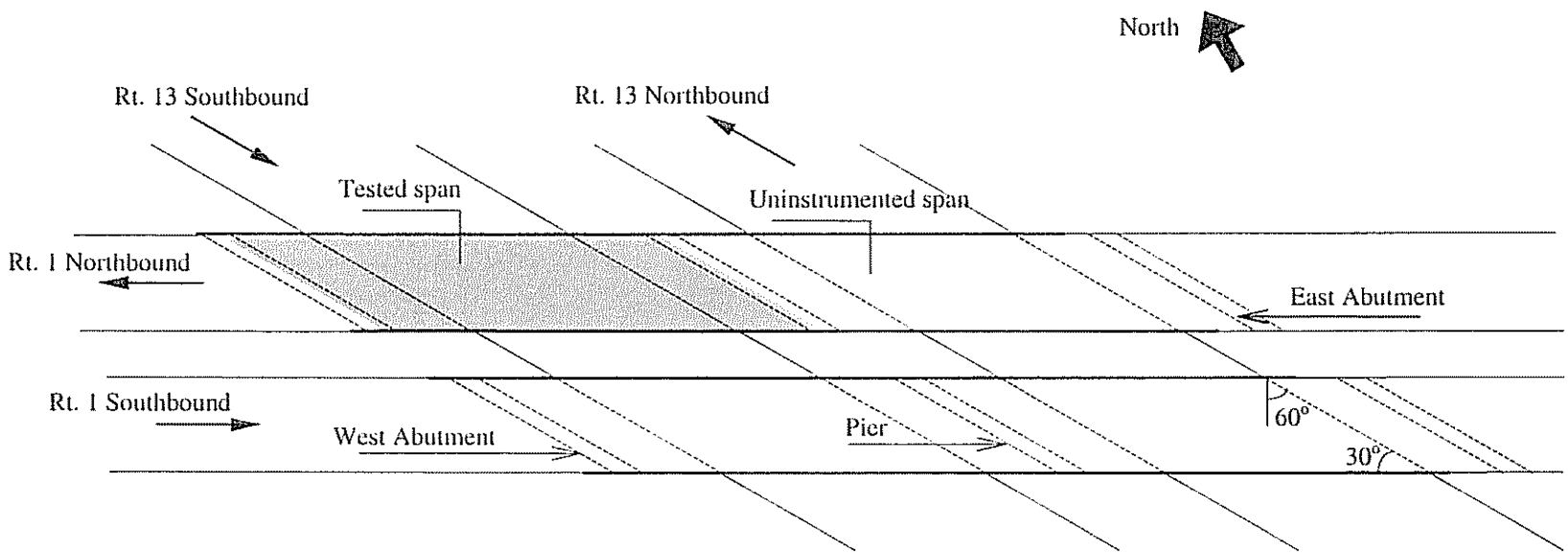

Figure 3.2.2 Plan view of the intersection

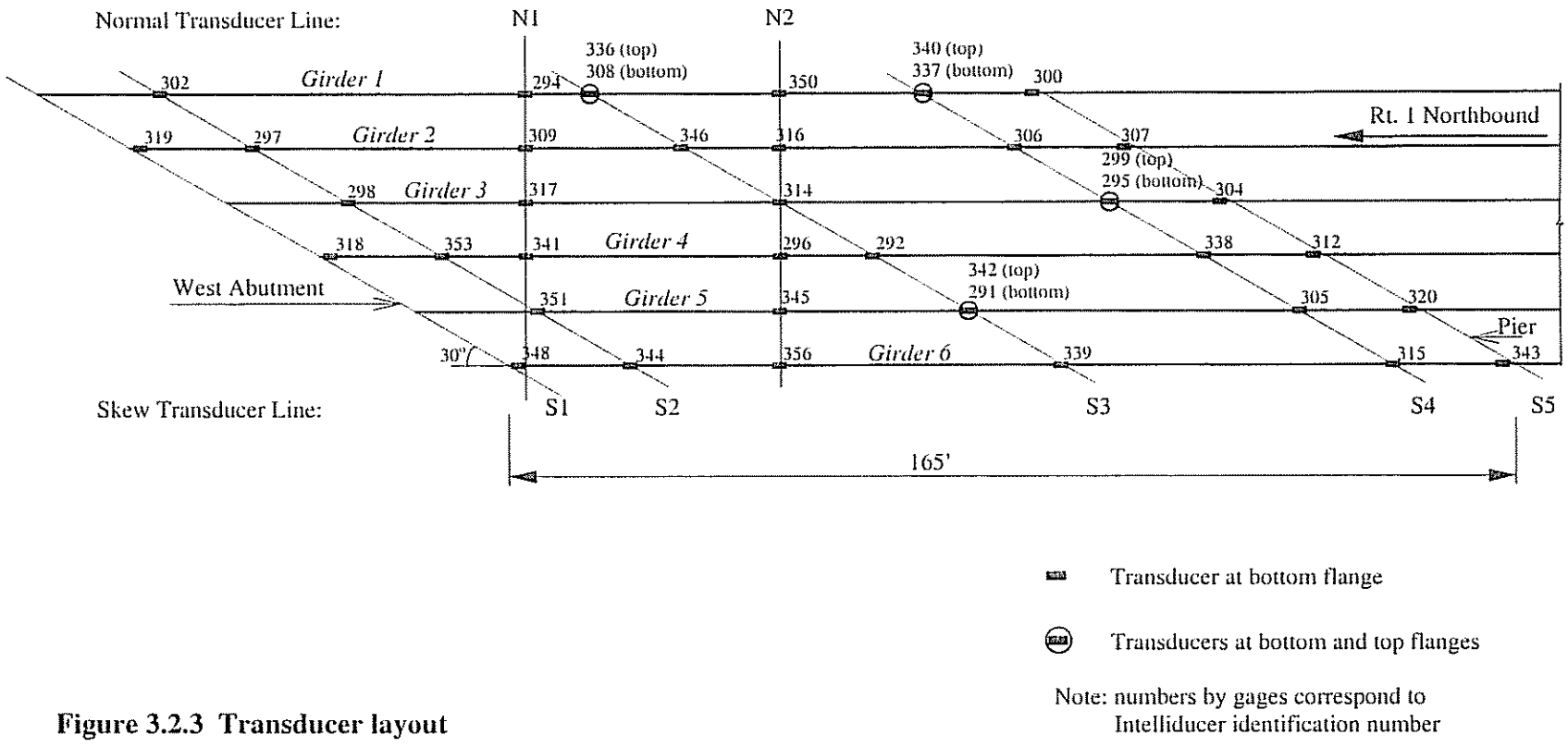

Figure 3.2.3 Transducer layout

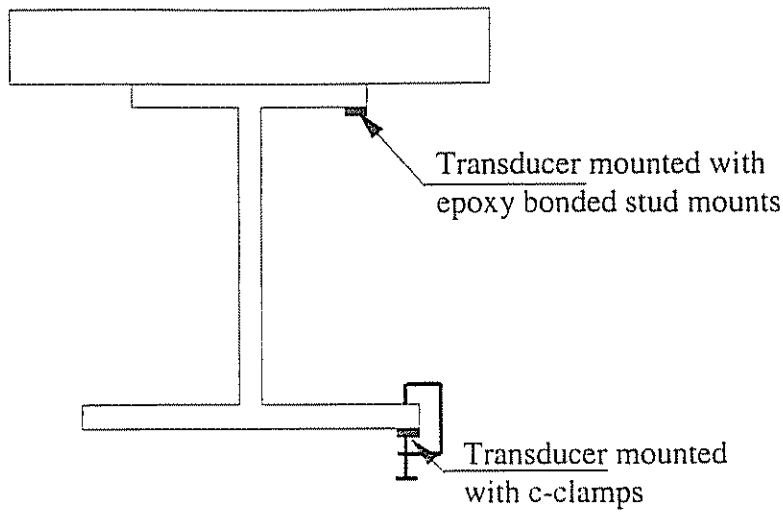

Figure 3.2.4 Sectional view

3.2.4 Loading

Two fully loaded ten-wheel dump trucks were used as the load for the test. The two trucks were identified by their vehicle numbers, #2844 and #2851. The three-axle vehicles were weighed on site and had the following gross vehicle weights: truck #2844, 60.95 Kips and truck #2851, 57.5 Kips. The axle spacings, dimensions and weights of truck wheels are shown in Figure 3.2.5.

3.2.5 Roadway Marking

Before the test was conducted the left, center and right lane lines of the roadway were divided into 10 foot longitudinal increments and marked as such with chalk. Marks were made on both spans of the bridge. These marks allow the location of the truck during the test to be identified.

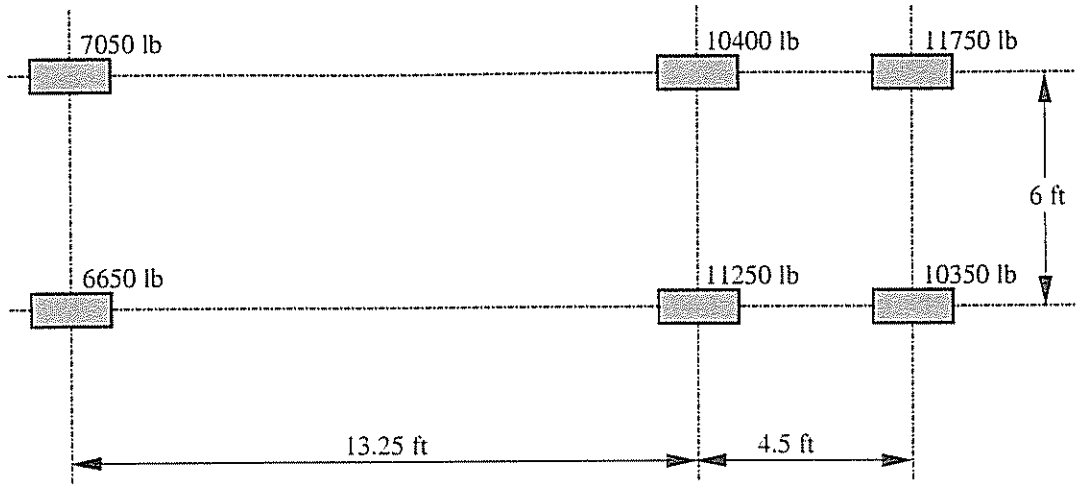

a. Dimension and weight of Truck 2851
(total weight 57.45 kips)

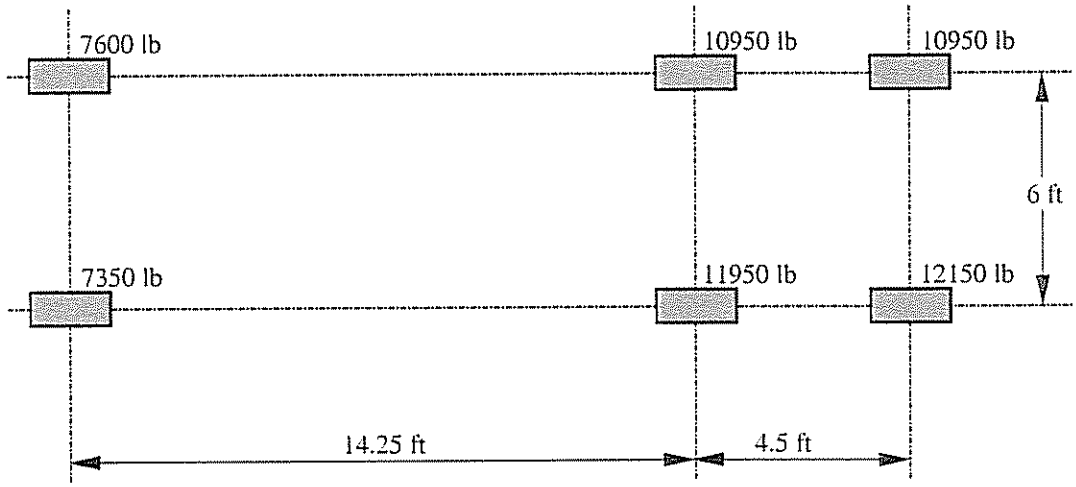

b. Dimension and weight of Truck 2844
(Total weight 60.95 kips)

Figure 3.2.5 Dimensions and weight distributions of load trucks

3.3 Test Procedure

A total of thirteen truck "passes" were made, each pass providing a separate and unique data set. During a typical pass one or both of the trucks traveled slowly across the bridge along a designated longitudinal line. The truck speed was on the order of 3 to 5 mph. A description of the thirteen passes is presented in Table 3.3.1. Nine of the passes were single truck passes on five different longitudinal lines. Four of the passes were dual truck passes on two different longitudinal lines. In the case of the latter, the vehicles crossed side-by-side at the same time. Presented in Figure 3.3.1 is a sketch of the truck passes. Strain data was recorded at a rate of 10 samples/second for all tests.

The longitudinal position of the truck was automatically recorded along with the strain data, using a radio transmitter. One person rode with the truck as it made its longitudinal pass. When the front wheel of the vehicle crossed a chalk mark on the roadway, the transmit button on the radio was pushed. The transmission was picked up by the main computer and a "mark" was recorded in the data. Knowing the spacing of the chalk marks (10 ft) and the sample rate, the exact position and speed of the truck could be determined for the entire test.

Note that since this was the northbound roadway, the trucks crossed from right to left on the diagrams (i.e., they were first on the uninstrumented span before crossing the instrumented span).

Table 3.3.1 Truck path of each pass

Pass number	Truck number	Truck path
1	2851	driver side wheel on the right line
2	2844	driver side wheel on the right line
3	2851	passenger side wheel on the right line
4	2844	passenger side wheel on the right line
5	2851	straddling the center line
6	2844	straddling the center line
7	2851	driver side wheel on the left yellow line
8	2844	driver side wheel on the left yellow line
9	2851	passenger side wheel on the left yellow line
10	2851	straddling the center line
	2844	driver side wheel on the right line
11	2851	passenger side wheel on the left yellow line
	2844	straddling the center line
12	2851	straddling the center line
	2844	driver side wheel on the right line
13	2851	passenger side wheel on the left yellow line
	2844	straddling the center line

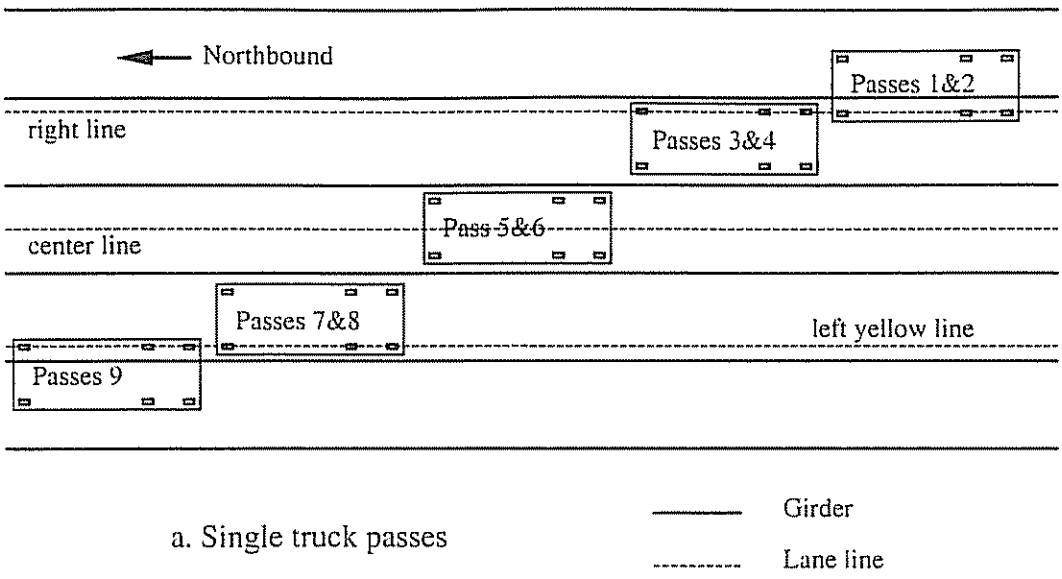

a. Single truck passes

Girder

Lane line

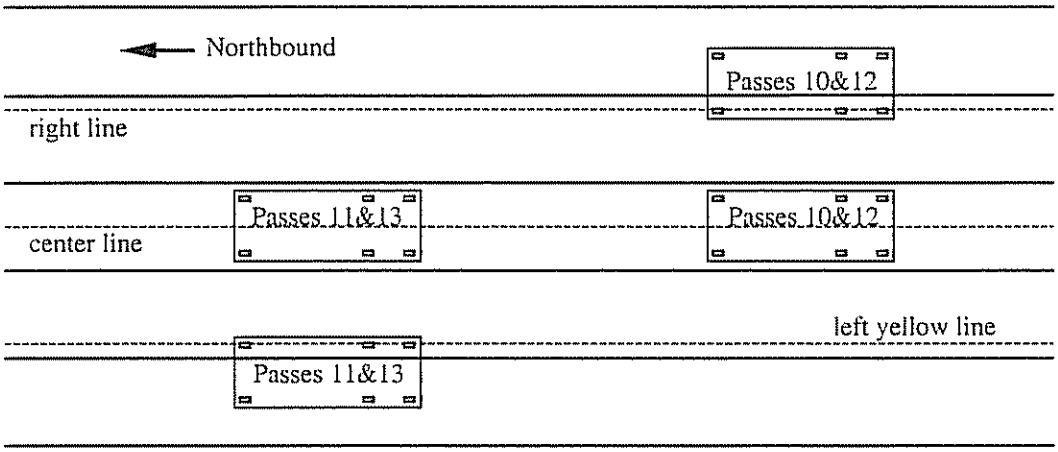

b. Dual truck passes

Girder

Lane line

Figure 3.3.1 Truck location of each pass

3.4 Test Results

A substantial amount of data was generated during the tests from the 40 transducers and 13 truck passes. Presented in the following are representative and key results from the test.

Presented in Figure 3.4.1 are typical strain time-histories for bottom flange gages from a single truck pass (#9). Note that positive strain indicates tension. Results are arranged by groups of transducers, along lines that are perpendicular to the girder (designated as N1 or N2) and parallel to the abutment (designated as S1 through S5). The transducer lines are shown in Figure 3.2.3. The results show a wide variation in strain history from one transducer to the next. In many cases the strain is initially negative, indicating negative bending, which would be expected since the truck was initially on the uninstrumented span. Otherwise, the strains vary greatly with the position of the transducer relative to the vehicle. Note that the maximum strain at transducer 356 is larger than the maximum strain at transducer 339, which is closer to the maximum moment point in a single girder. It may be due to the skew geometry, in which transducer 339 is closer to the support.

The absolute maximum positive and negative strains from each pass are shown in Table 3.4.1. Locations of maximum strains, i.e., transducer number, and locations of the truck, i.e., distance from the west abutment of the bridge, are also shown. The distance was measured along the left, center or right line from the west abutment of the tested span of the bridge to the front wheel of the truck.

For the one truck passes, the maximum positive strain recorded was 72 με and the maximum negative strain was 38 με. Both of these maximum strains occurred during pass 1 (driver side wheel on the right line) and in the edge girder. For

the dual truck passes, the maximum positive strain recorded was 94 με and the maximum negative strain was 48 με. The maximum positive strains for the two truck passes were all nearly equal and varied between 90 and 94 με. The maximum positive strains always occurred in the edge girder (i.e., girder 1 or 6) or one girder in from the edge (i.e., girder 2 or 5).

Contour plots of strain for passes 2, 5 and 9 are shown in Figures 3.4.2, 3.4.3, and 3.4.4 respectively. The contour plots were generated using MATLAB. A Fortran program was developed to read the test data, arrange the data needed for contour plots and output an M-file for MATLAB. The results of running the M-file in MATLAB were the contour plots.

Contour plots are shown for the truck in four different positions: when the maximum strain was reached, and when the truck was at the quarter, center and three-quarter points of the instrumented span. The location of the truck for each plot is shown in the figure as a dashed lined box. The dashed line represents the applicable traffic line for the pass, i.e., the right line, the center line and the left yellow line. The plots show that the strain (load) distribution is more or less parallel to the skew line. Also, the load is carried mostly by the girders directly beneath the truck, i.e., the distribution of load is fairly narrow.

Although the girders are "pinned" at the ends, negative moments were measured at the obtuse corner near the abutment. One possible explanation for the negative moments at the pinned ends might be that the bearings are not perfect pins, i.e., there is some constraint on rotation. Another reason may be bridge skew and diaphragms, as discussed in Chapter 4.

The strain distributions along each girder when the peak strain occurred, for passes 2, 5 and 9, are shown in Figure 3.4.5. For passes 2 and 9, the maximum strain occurred in girder 2 and girder 5 respectively, which were located directly beneath the load truck. For pass 5, the maximum strain occurred in girders 3 and 4, while the load was between girders 3 and 4. It shows that the maximum strain appeared in the girders near the load, regardless the load location, i.e., the girders near the load carried most of the load.

The transverse distribution factor for moment for each girder is shown in Table 3.4.2. The distribution factor (DF) is defined as the ratio of the maximum measured moment in a girder during a pass, divided by the maximum theoretical moment determined by applying the entire load truck to a single composite girder. For positive moment, the measured load distribution factors for a single lane loaded and two lanes loaded are significantly smaller than those given by the AASHTO load distribution formulas (1.1 through 1.4). For the edge girder and a single lane loaded, the AASHTO formula predicts a DF of 0.57 while the tests indicate a maximum value of 0.29. For interior girders and a single lane loaded, the AASHTO formula predicts a DF of 0.36 while the tests indicate a maximum value of 0.26. For two lanes loaded the AASHTO formula predicts a DF of 0.54 and the tests indicate a maximum value of 0.39. For negative moment, the measured load distribution factors for a single lane loaded and two lanes loaded are close to those predicted by the AASHTO formulas (1.1 through 1.4). For the edge girder and a single lane loaded, the AASHTO formula predicts a DF of 0.56 while the tests indicate a maximum value of 0.46. For interior girders and a single lane loaded, the AASHTO formula predicts a DF of 0.37 while the tests indicate a maximum value of 0.39. For two lanes loaded the AASHTO formula

predicts a DF of 0.56 and the tests indicate a maximum value of 0.58. In general, the AASHTO DF formulas are conservative, in some cases by as much as a factor of 2. It shows that the skew effect has different influence on positive and negative moments. The skew yields smaller positive moments than predicted and larger negative moments than predicted. The AASHTO specifications provide one load distribution factor regardless the location of moments in a continuous bridge, i.e., inside a span or at middle support.

The neutral axis location of the girders, considering the composite effect of the deck, were calculated using the strains from the four pairs of transducers that were located on the top and bottom flanges at the same locations, as shown in Figure 3.2.3. For these calculations, plane strain distributions were assumed. The theoretical locations of the neutral axis at these locations were also calculated by considering the full composite effect. The theoretical and experimental neutral axis locations are shown in Table 3.4.3. The experimental neutral axis locations listed in the table were the averages of a period around peak strain. The measured locations are in close agreement with the theoretical locations, indicating that the girders and the deck are fully composite.

A comparison of the strains from pass 11, with the superposition of passes 5 and 9 is shown in Table 3.4.4. Because small strains are susceptible to experimental error, strains less than 15 Microstrains were not included in the comparison. The absolute relative differences range from 1.7% to 31.1%, with an average value of 13.6%. These results demonstrate that the bridge is behaving linearly and that superposition of the measured strains is justifiable.

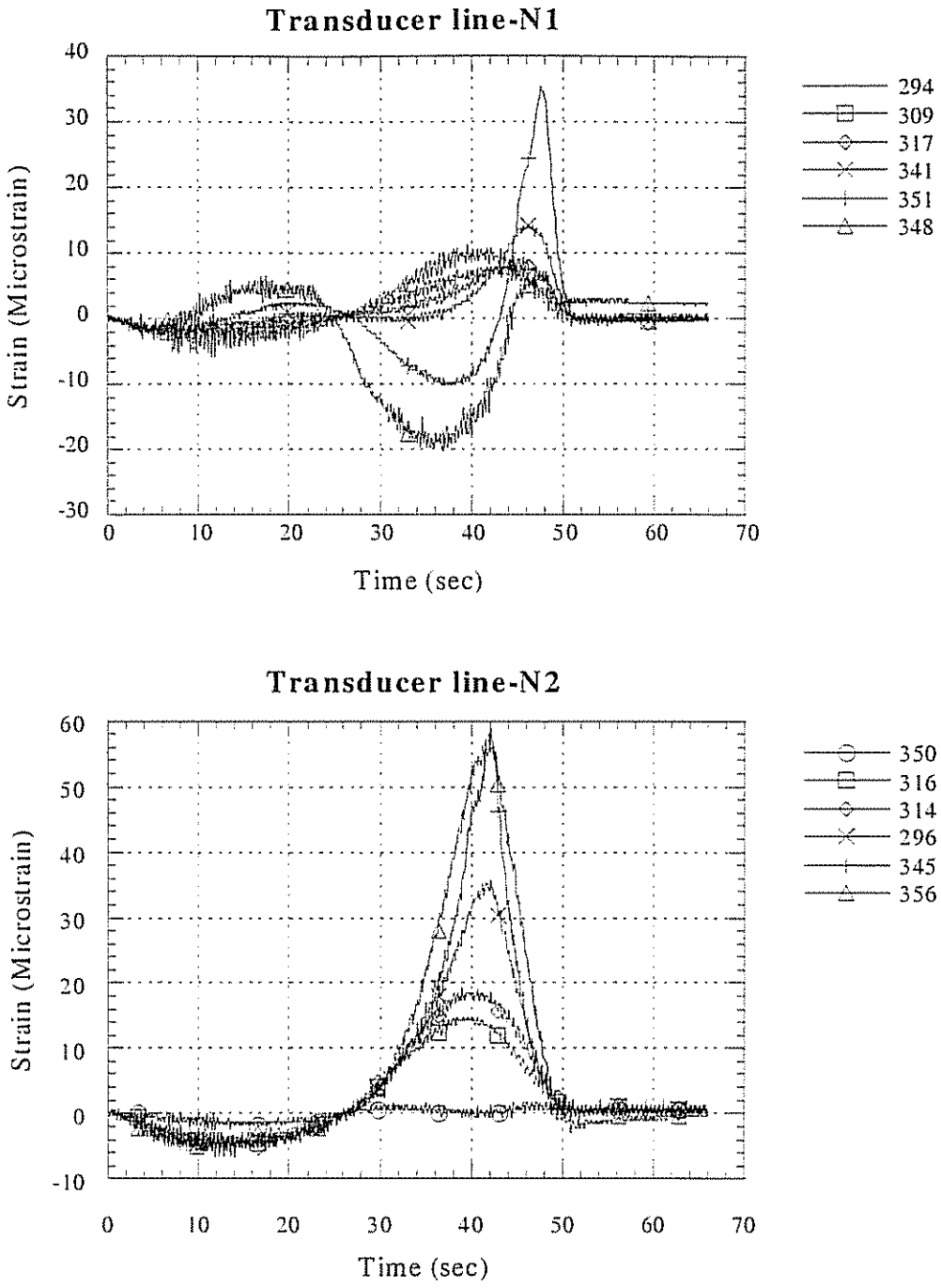

Figure 3.4.1 Time history of strains for pass 9

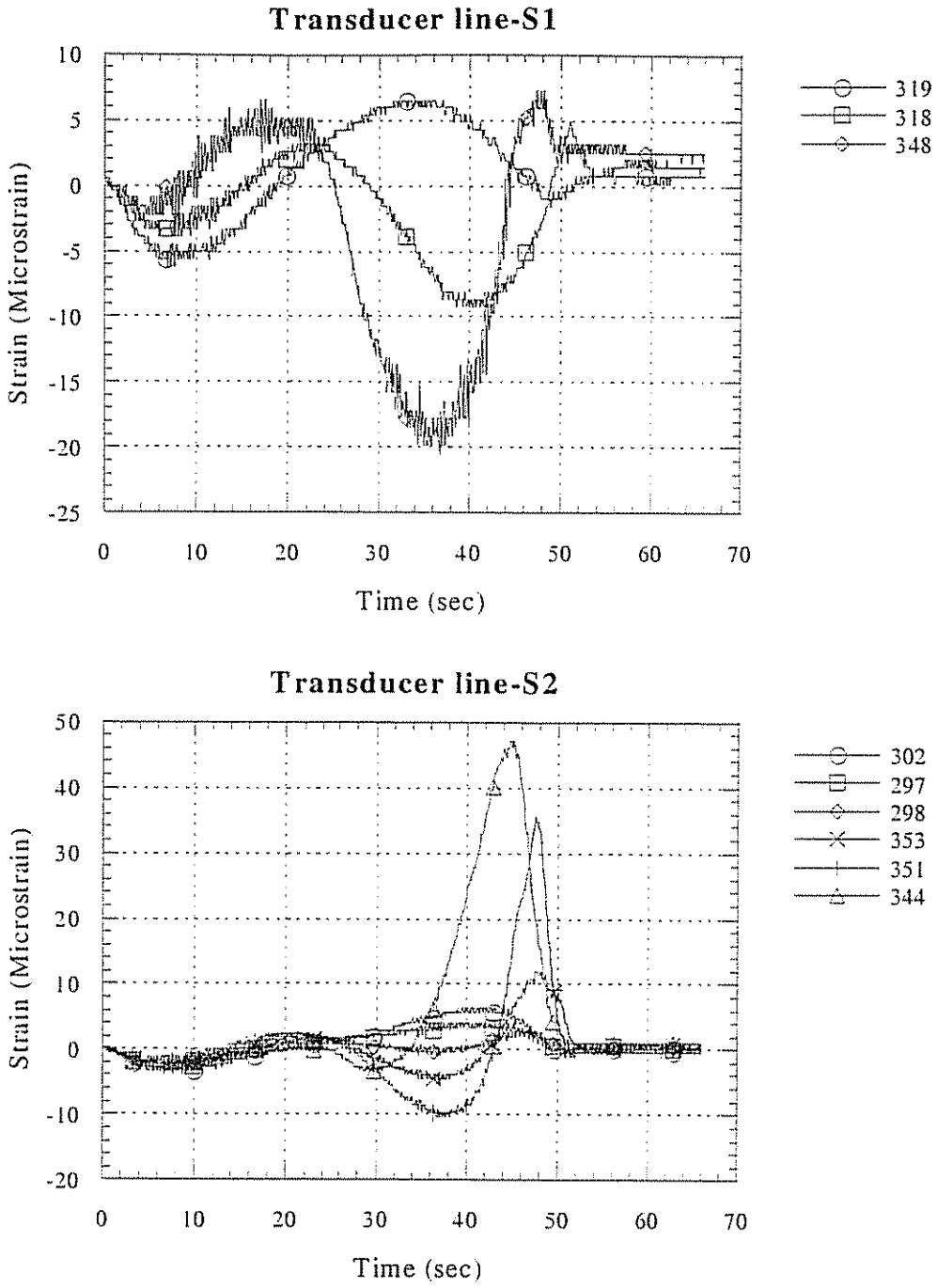

Figure 3.4.1 (continued) Time history of strains for pass 9

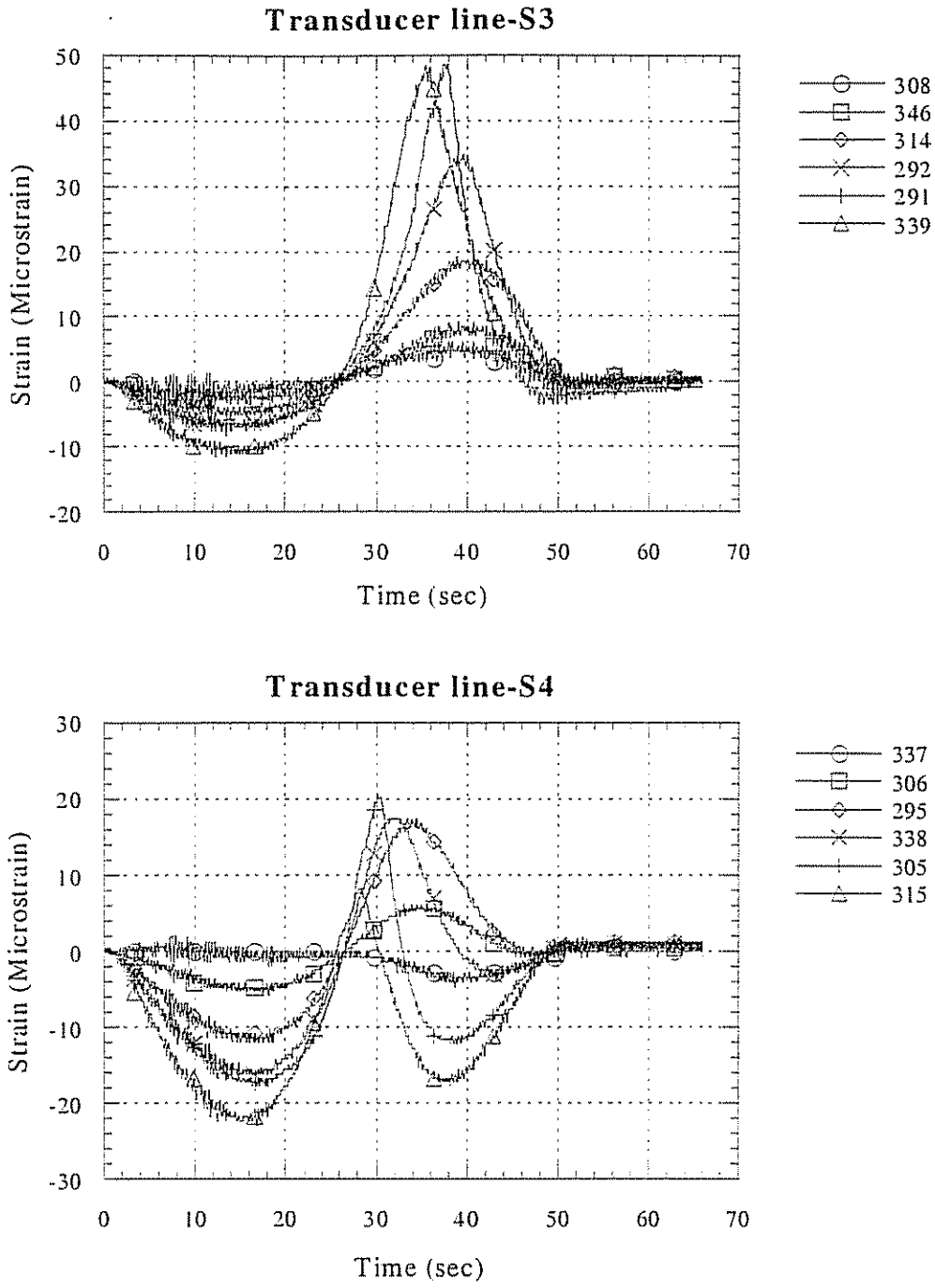

Figure 3.4.1 (continued) Time history of strains for pass 9

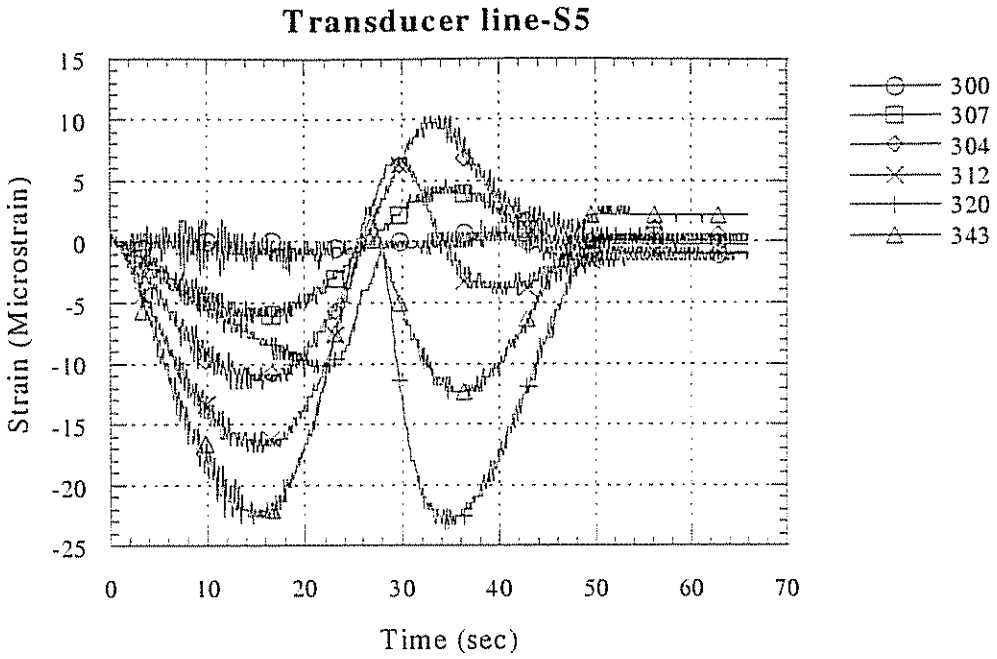

Figure 3.4.1 (continued) Time history of strains for pass 9

Table 3.4.1 Peak positive and negative strains for each pass and the corresponding truck location

Pass number	ε^{+}_{max} (με)	Transducer number	Distance (ft)	ε^{-}_{max} (με)	Transducer number	Distance (ft)
1	72	294	50.8	-38	300	73.6
2	65	294	47.1	-36	300	72.0
3	49	314	47.1	-24	348	78.8
4	51	309	48.6	-28	348	75.6
5	52	314	67.5	-22	348	70.7
6	57	296	64.3	-23	348	69.3
7	54	296	49.2	-21	348	72.3
8	56	296	57.9	-22	348	92.3
9	59	345	46.4	-24	320	102.9
10	92	294	61.3	-48	300	85.6
11	91	345	67.7	-35	315	90.7
12	90	309	37.3	-47	300	60.0
13	94	345	74.7	-30	348	105.3

(ε^{+}_{max} is the maximum positive strain and ε^{-}_{max} the maximum negative strain. Distance is measured from the west abutment to the front wheel of the truck.)

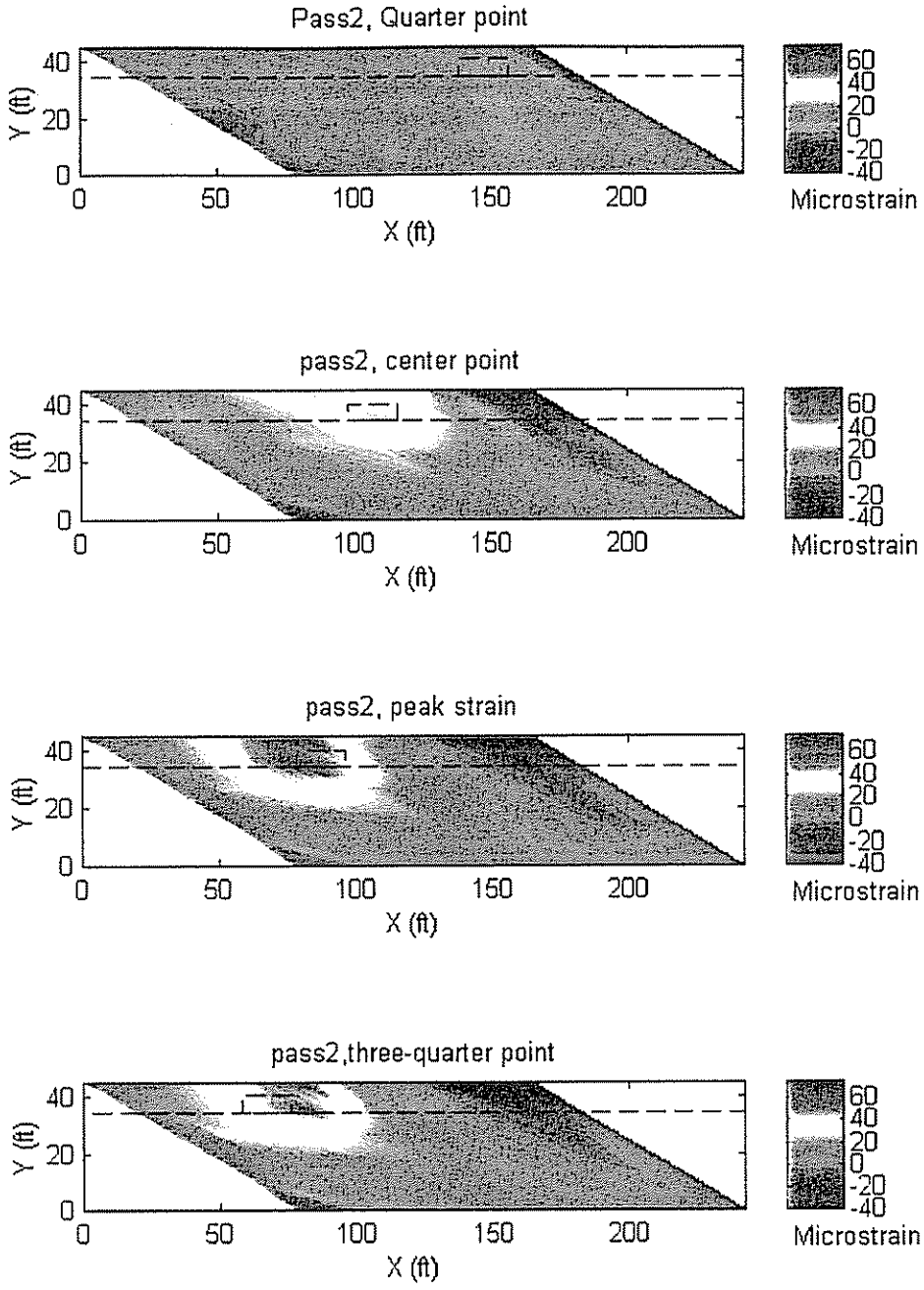

Figure 3.4.2 Contour plots of strains for pass 2

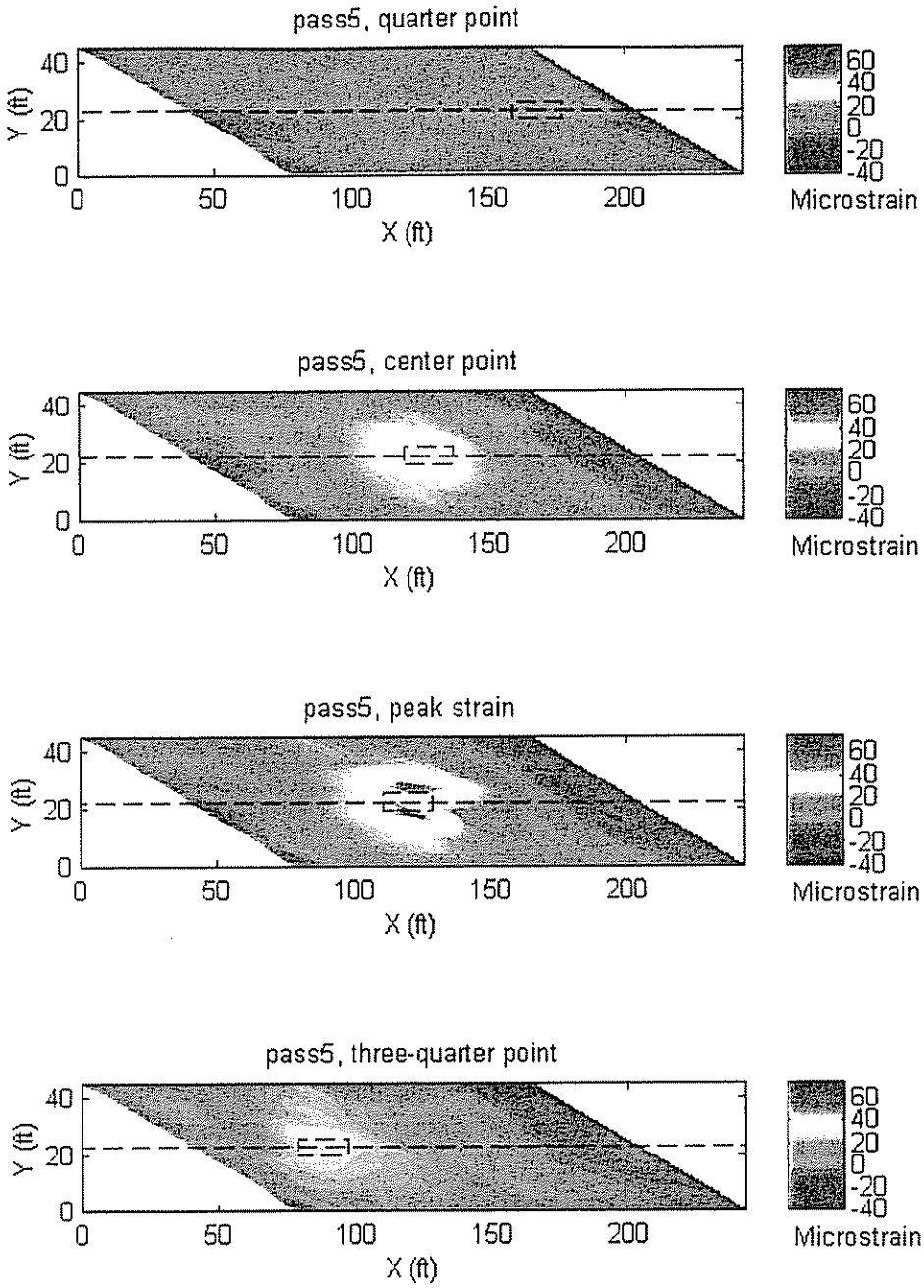

Figure 3.4.3 Contour plots of strains for pass 5

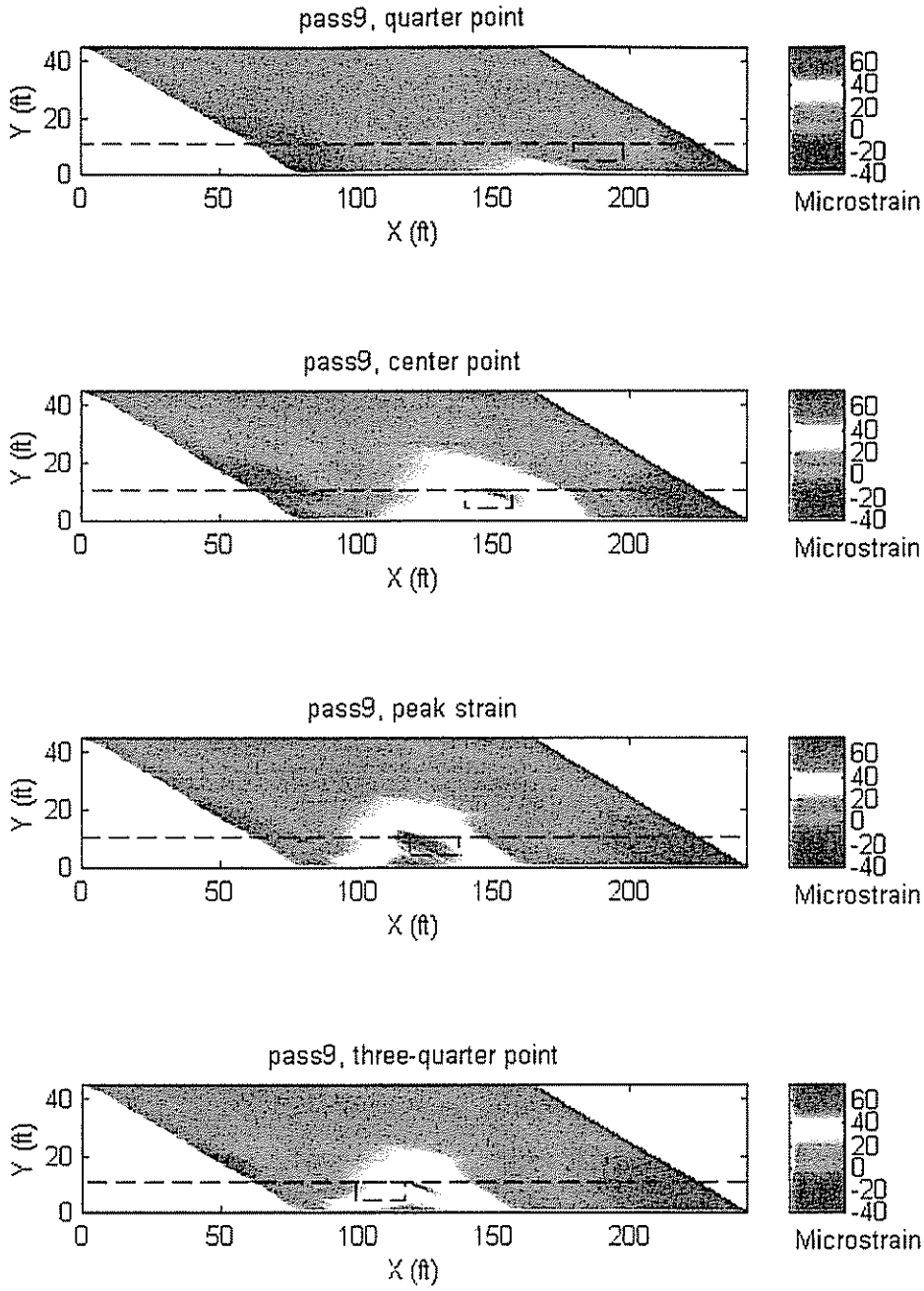

Figure 3.4.4 Contour plots of strains for pass 9

a. Girder 1

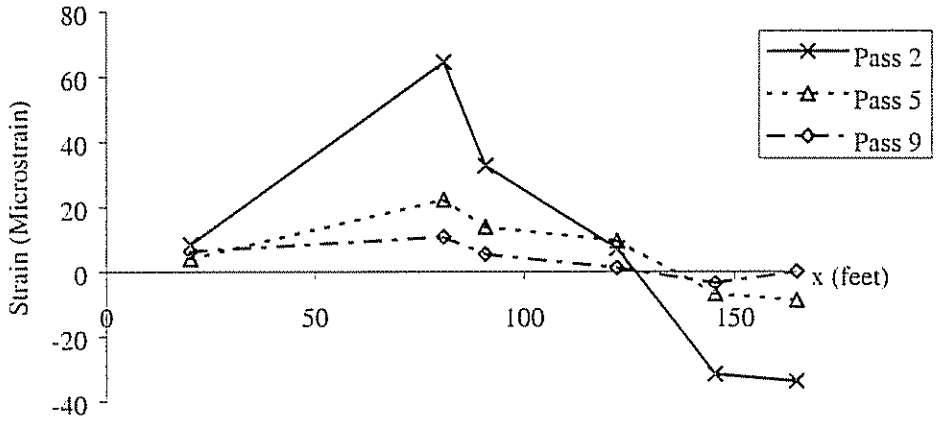

b. Girder 2

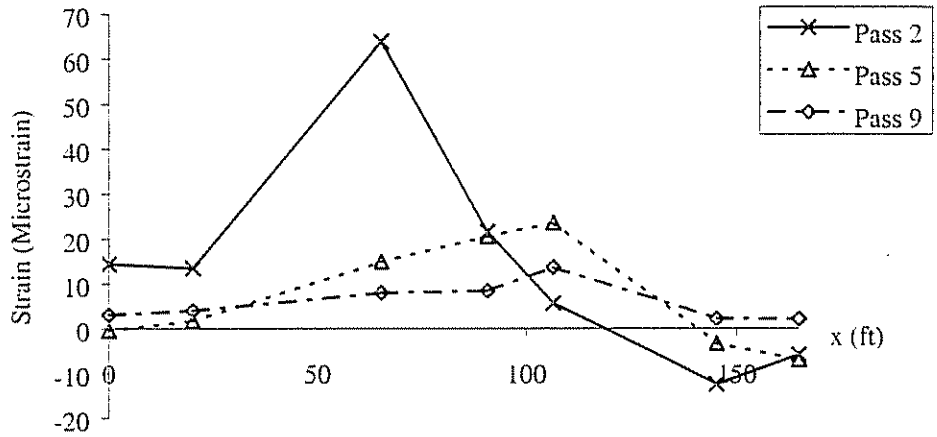

Figure 3.4.5 Strain distribution along girders at peak strain

c. Girder 3

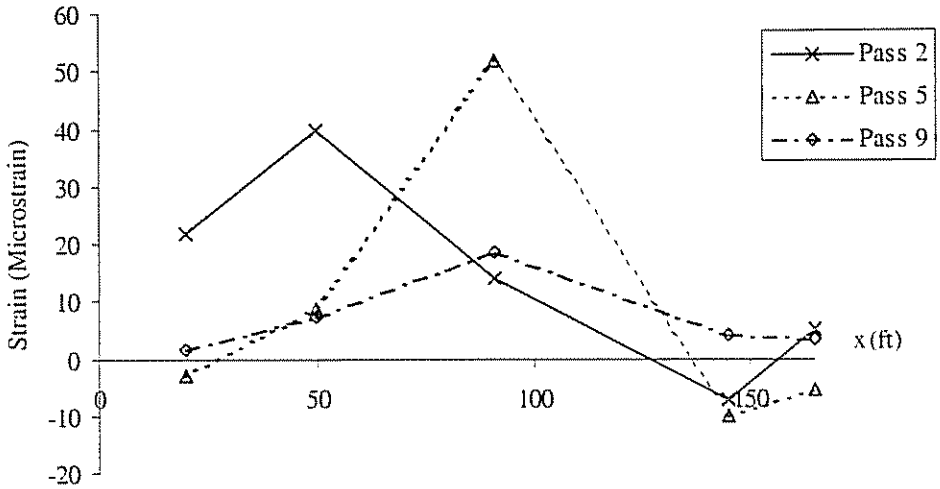

d. Girder 4

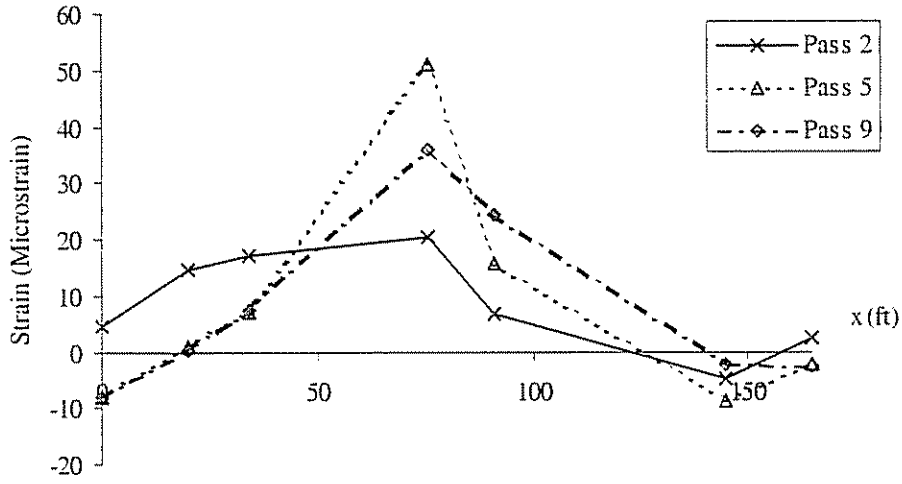

Figure 3.4.5 (continued) Strain distribution along girders at peak strain

e. Girder 5

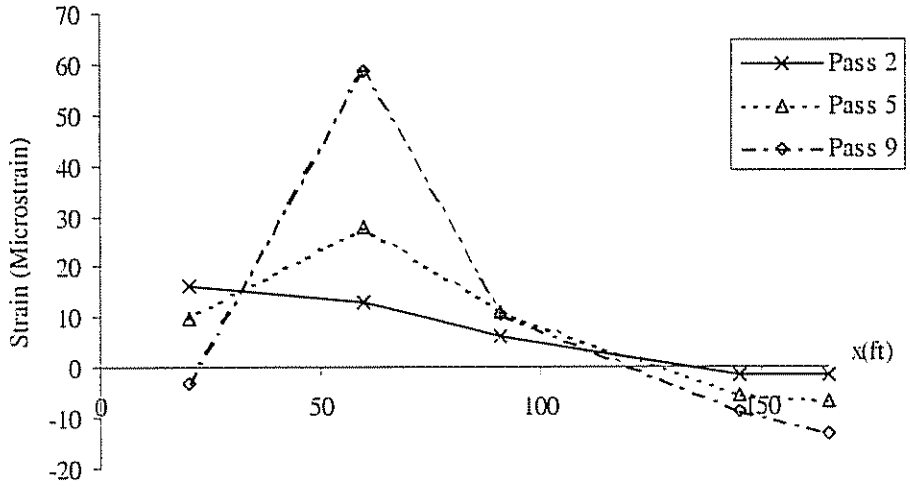

f. Girder 6

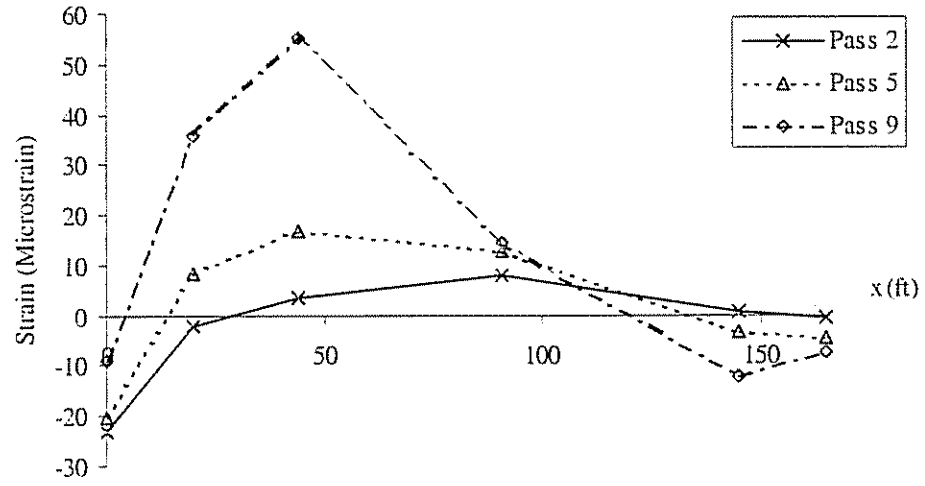

Figure 3.4.5 (continued) Strain distribution along girders at peak strain

Table 3.4.2 Load distribution factor for moment

Single truck passes						
pass number	load distribution factor for positive moment					
	Girder 1	Girder 2	Girder 3	Girder 4	Girder 5	Girder 6
1	**0.29**	0.26	0.15	0.09	0.06	0.05
2	0.26	**0.26**	0.16	0.10	0.06	0.05
3	0.16	0.18	0.20	0.13	0.08	0.05
4	0.18	0.21	0.20	0.12	0.08	0.05
5	0.09	0.10	**0.21**	0.21	0.11	0.07
6	0.09	0.10	0.20	**0.24**	0.13	0.08
7	0.07	0.07	0.12	0.22	0.20	0.17
8	0.06	0.08	0.13	0.23	0.21	0.15
9	0.05	0.06	0.08	0.15	**0.24**	**0.24**
Max	**0.29**	**0.26**	0.21	0.24	0.24	0.24
AASHTO	**0.57**	**0.36**	0.36	0.36	0.36	0.57
pass number	load distribution factor for negative moment					
	Girder 1	Girder 2	Girder 3	Girder 4	Girder 5	Girder 6
1	**0.46**	**0.39**	**0.38**	0.23	0.10	0.15
2	0.44	0.36	0.37	0.23	0.11	0.13
3	0.26	0.23	0.29	0.22	0.12	0.12
4	0.31	0.25	0.30	**0.23**	0.13	0.14
5	0.14	0.14	0.20	0.21	0.15	0.11
6	0.14	0.15	0.20	0.23	0.17	0.12
7	0.07	0.11	0.17	0.21	0.19	0.16
8	0.06	0.11	0.17	0.22	0.21	0.18
9	0.04	0.08	0.15	0.21	**0.29**	**0.28**
Max	**0.46**	**0.39**	0.38	0.23	0.29	0.28
AASHTO	**0.56**	**0.37**	0.37	0.37	0.37	0.56

Table 3.4.2 (continued) Load distribution factor for moment

Dual truck passes						
pass number	load distribution factor for positive moment					
	Girder 1	Girder 2	Girder 3	Girder 4	Girder 5	Girder 6
10	**0.37**	**0.37**	0.34	0.31	0.18	0.10
11	0.14	0.16	0.29	0.38	0.38	**0.36**
12	0.37	0.37	**0.34**	0.30	0.18	0.09
13	0.14	0.16	0.29	**0.38**	**0.39**	0.35
Max	0.37	0.37	0.34	0.38	**0.39**	0.36
AASHTO	0.54	0.54	0.54	0.54	**0.54**	0.54
pass number	load distribution factor for negative moment					
	Girder 1	Girder 2	Girder 3	Girder 4	Girder 5	Girder 6
10	**0.58**	**0.48**	0.55	0.41	0.24	0.21
11	0.16	0.22	0.33	0.36	**0.40**	**0.39**
12	0.57	0.47	**0.55**	**0.42**	0.24	0.22
13	0.15	0.19	0.30	0.28	0.36	0.29
Max	**0.58**	0.48	0.55	0.42	0.40	0.39
AASHTO	**0.56**	0.56	0.56	0.56	0.56	0.56

Table 3.4.3 Locations* of neutral axis (inch)

Pass	Transducers			
	336-308	342-291	299-295	340-337
1	50.09	54.48	48.82	55.29
2	48.38	56.98	52.89	55.82
3	44.58	54.53	61.00	53.89
4	45.74	54.70	60.28	52.84
5	46.22	54.60	60.83	47.57
6	46.25	55.61	61.81	46.51
7	47.21	57.26	61.81	48.08
8	47.74	57.56	61.31	56.96
9	46.57	57.30	56.92	58.17
10	49.07	58.07	57.89	53.70
11	46.35	58.50	59.54	56.84
12	50.06	56.61	58.54	53.87
13	45.84	57.50	59.68	57.93
Average	47.24	56.44	58.56	53.65
Theoretical	54.39	56.65	55.86	53.79
δ (%)**	15.1	0.4	-4.6	0.3

*: Location of neutral axis is measured from the bottom of the bottom flange.
**: δ is relative difference =(theoretical-experimental)/experimental.

Table 3.4.4 Comparison of strains (in Microstrain) of dual truck pass with the superposition of single truck passes

Transducer	Pass 5	Pass 9	Pass 5 + Pass 9	Pass 11	δ (%)
308	12.7	6.0	18.7	17.5	7.09
309	10.5	8.0	18.4	22.6	-18.38
294	18.1	10.7	28.8	31.5	-8.57
302	3.5	6.3	9.8	12.5	-21.16
344	7.9	27.2	35.1	50.9	-31.06
356	16.2	53.1	69.3	82.7	-16.26
314	42.6	19.2	61.8	67.0	-7.78
296	41.5	33.5	75.0	88.4	-15.13
345	26.1	47.8	73.8	82.7	-10.75
346	18.1	9.1	27.1	27.9	-2.69
291	13.9	19.2	33.1	35.8	-7.64
339	13.6	20.6	34.2	38.1	-10.26
292	27.4	31.8	59.2	52.2	13.27
305	-5.6	-10.0	-15.6	-12.5	25.13
315	-2.8	-13.9	-16.7	-15.1	10.46
320	-7.4	-15.8	-23.2	-24.9	-6.60
316	22.5	14.8	37.3	37.9	-1.67
317	4.8	6.8	11.6	16.8	-30.69

δ: relative difference = (pass 5 + pass 9 – pass 11) / pass11

Chapter 4

MODELING AND ANALYSIS

4.1 Introduction

A three-dimensional finite element model of the bridge was developed using the commercial program ANSYS, (Release 5.3). The ANSYS program is a general-purpose finite element program that can be used to solve structural, mechanical, electrical, electromagnetic, thermal, fluid, and biomedical problems. For structural applications, analysis options include static, modal, harmonic, transient dynamic, spectrum, and buckling analyses. The primary unknowns (nodal degrees of freedom) calculated in a structural analysis are displacements. Other quantities, such as strains, stresses, and reaction forces, are derived from the nodal displacements.

Three-dimensional elastic shell elements, which accounted for in-plane and out-of-plane plate behavior of the reinforced concrete deck were used in the analysis. Three-dimensional elastic beam elements were used to model the steel girders. The diaphragm cross frames were simplified and modeled using beam elements with the equivalent stiffness of the diaphragm. The composite action between the deck and the girders was modeled using rigid connections and constraint equations. The bearings were modeled using two methods: (1) a simple beam support, and (2) a more detailed model of the actual bearing. The overhang of the bridge was ignored in the analyses.

Two trucks, one straddling the center line and the other passing with the driver side wheel on the left yellow line, were used as the loads. The truck location used was that which caused the peak strain during the test for pass 11.

The influence of mesh size was studied to determine the degree of refinement needed to obtain accurate results. The effect of transverse stiffness on the load distribution among girders, i.e., influences of the elastic modulus of the concrete deck, and the effect of the diaphragms was studied. Two methods of modeling the bearings were compared.

Finally, the analysis results were compared with the test results and with the results obtained using the load distribution method of AASHTO.

4.2 Modeling

4.2.1 Overview

The bridge was modeled using a combination of beam elements for the girders and shell elements for the concrete deck. The nominal spacing of nodes in the girders was 0.5 ft and in the deck, 1.0 ft. Composite action between the steel girders and the concrete deck was modeled using constraint equations. The support conditions were imposed directly on the end nodes of the girders: the ends of girders were considered to be supported by rollers whose movement in the x direction was free and the intermediate girder supports were pinned. The transverse diaphragms were simplified and modeled using beam elements. The overhang and parapet were ignored in the analyses.

The finite element model of the bridge is shown in Figures 4.2.1 and 4.2.2.

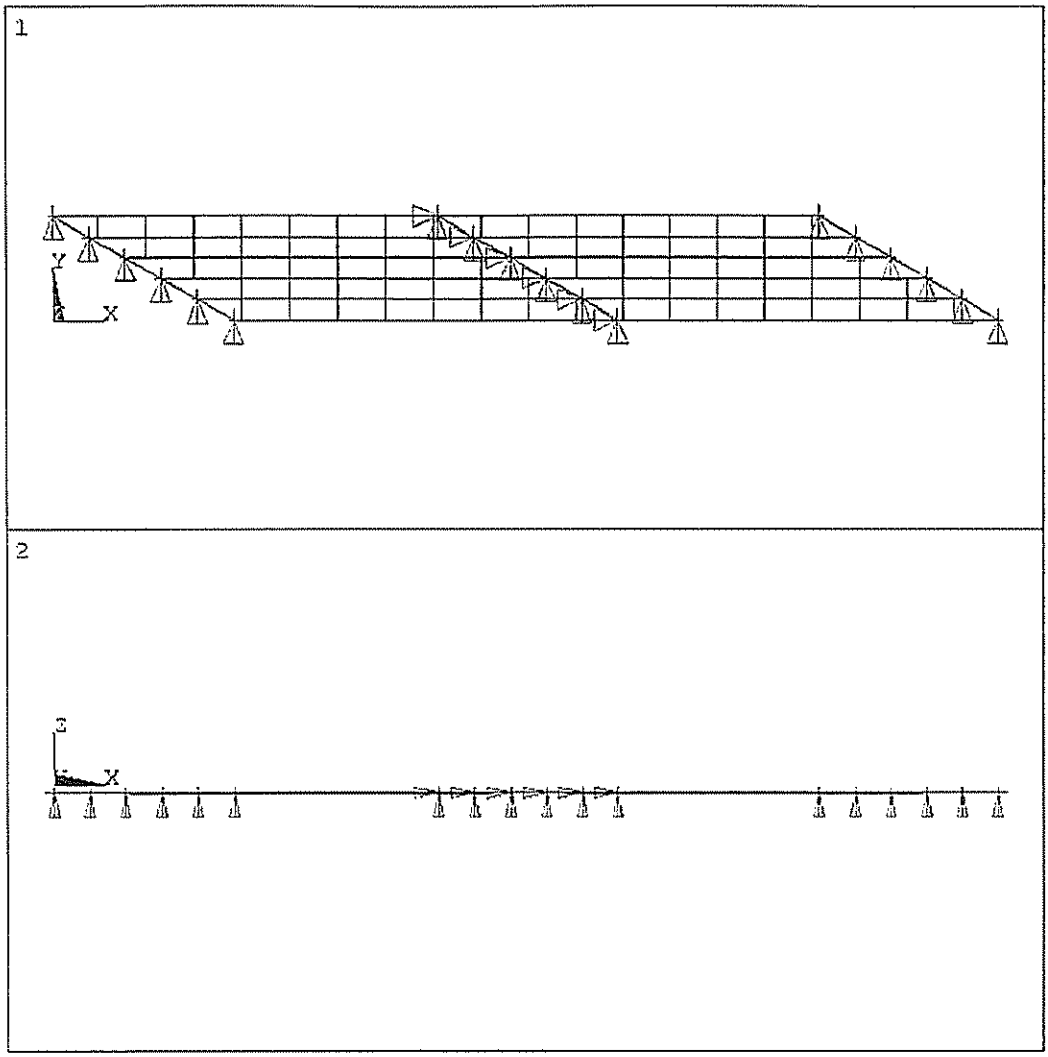

Figure 4.2.1 Finite element model of the girders and transverse diaphragms

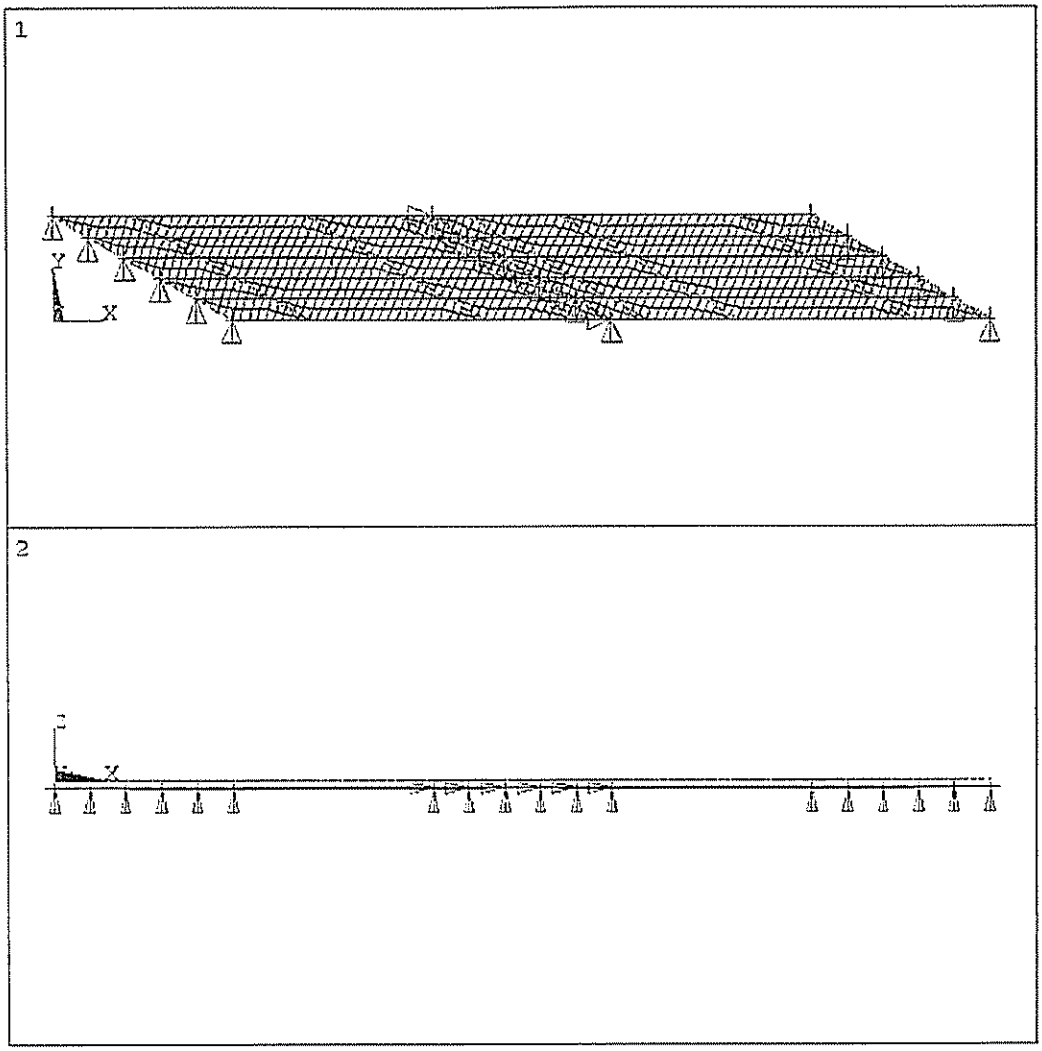

Figure 4.2.2 Finite element model of the deck and girders

4.2.2 Modeling of Slab

The concrete slab was modeled using a four-node three-dimensional elastic shell elements. The elements have both bending and membrane capabilities; both in-plane and normal loads are permitted. The element has six degrees of freedom at each node: translations in the nodal x, y, and z directions and rotations about the nodal x, y, and z axes. Loads may be input as surface pressures on the six element faces.

Each element was defined by four nodes, four thicknesses (one at each node), and the isotropic material properties. Thickness of the element was assumed to be a constant nine inches, at all four nodes. The elastic modulus of the concrete was calculated from the concrete strength specified in the construction drawings ($f_c^{'} = 4{,}500\,\text{psi}$). This corresponds to a modulus for the concrete of 3,824 ksi.

4.2.3 Modeling of Girders

The steel girders of the bridge were modeled using two-node three-dimensional elastic beam elements, as shown in Figure 4.2.3.

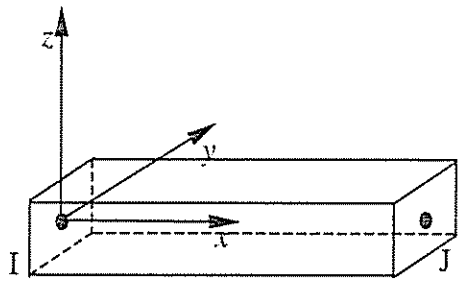

Figure 4.2.3 Beam element

The beam element is a uniaxial element with tension, compression, bending in y and z directions, and torsion capabilities. The element has six degrees of freedom at each node: translations in the nodal x, y, and z directions and rotations about the nodal x, y, and z axes. Pressures may by input as surface loads.

The element is defined by two nodes, the cross-sectional area (A), two area moments of inertia (I_y and I_z in y and z directions), two thicknesses (in y and z directions), the torsional moment of inertia (in x direction), and the material properties. The element can have any cross-sectional shape for which the moments of inertia can be computed. The thickness was used only in the bending stress calculations, in which the stresses were determined as if the distance between the neutral axis and the extreme fiber is one-half of the corresponding thickness.

Referring to Figure 2.2, the section properties of the girders varied along their length: properties of the four different sections are shown in Table 4.2.1. The elastic modulus for the girder beam elements was 29,000 ksi. The sectional properties of beam elements, A, I_y, and I_z, were calculated from the girder sections. The torsional moment of inertia, I_x, was assumed equal to the polar moment of inertia ($I_y + I_z$). The sectional properties for diaphragms were calculated from the cross-frames, as described later.

Table 4.2.1 Sectional properties of the four different sections of girders

Section	top flange		web		bottom flange		Area	I_y	I_z
	b_t (in)	t_t (in)	b_w (in)	t_w (in)	b_b (in)	t_b (in)	(in^2)	(ft^4)	(ft^4)
1	14	1	66	9/16	18	1	69.13	2.37	0.035
2	14	1	66	9/16	18	1 3/4	82.63	2.94	0.052
3	18	1 5/8	66	11/16	20	1 3/4	109.63	4.33	0.094
4	30	1 3/4	66	11/16	30	2	157.88	7.03	0.407

4.2.4 Modeling of Composite Action

As shown in Figure 2.4, the slab and the girders were designed to work compositely, due to the shear studs between the deck and girders. The field test results verified the composite action, as noted by the results in Table 3.4.3. To model the composite action, constraint equations were used between the deck element degrees of freedom and the girder element degrees of freedom.

A composite beam and slab is shown in Figure 4.2.4(a). Note that the nodes defining the girder beam elements are located at the centroid of the girder cross section, and the nodes defining the deck shell elements are located at the mid-height of the slab. With full composite action, there is a relationship between slab and girder deformations, which can be expressed as

$$u_{Jx} = u_{Ix} + d\sin(\theta_y) \tag{4.2.1}$$

$$u_{Jy} = u_{Iy} - d\sin(\theta_x) \tag{4.2.2}$$

$$u_{Jz} = u_{Iz} \tag{4.2.3}$$

$$\theta_{Jx} = \theta_{Ix} \tag{4.2.4}$$

$$\theta_{Jy} = \theta_{Iy} \tag{4.2.5}$$

$$\theta_{Jz} = \theta_{Iz} \tag{4.2.6}$$

Nodes I and J are nodes in the beam and slab respectively, and in the same vertical line. In the formulas, u is translation and θ is rotation, d is the distance between nodes I and J, and the first letter in the subscript denotes the node and the second one denotes the direction of the deformation. In the model, this relationship was defined for all nodes at the deck/girder interface.

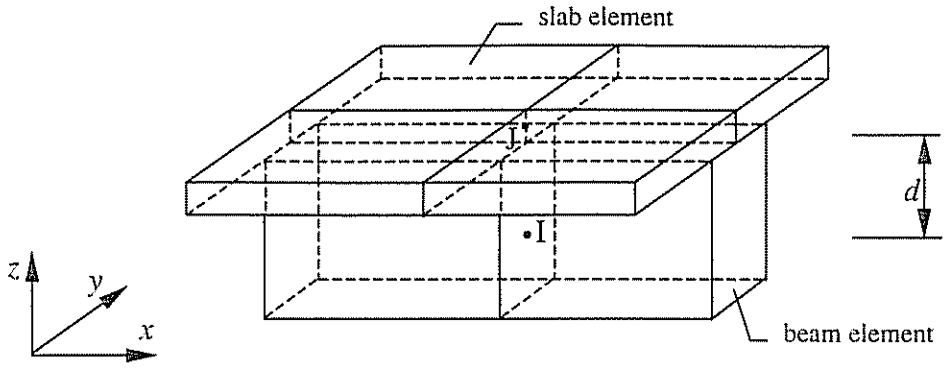

a. The shell element and the beam element

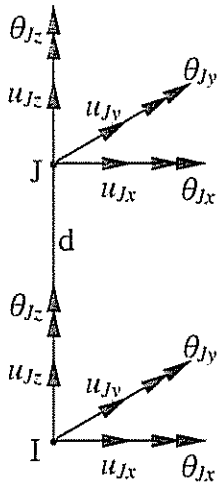

b. Nodal degrees of freedom

Figure 4.2.4 Composite action between beam and slab

4.2.5 Modeling of Girder Section Changes

The girder section in the bridge varies longitudinally, as discussed in Section 4.2.3. In modeling the girders, beam elements were placed at the centroids of the girders; however, because of the differences in section depth the centroids of the various sections were not on the same line, as shown in Figure 4.2.5.

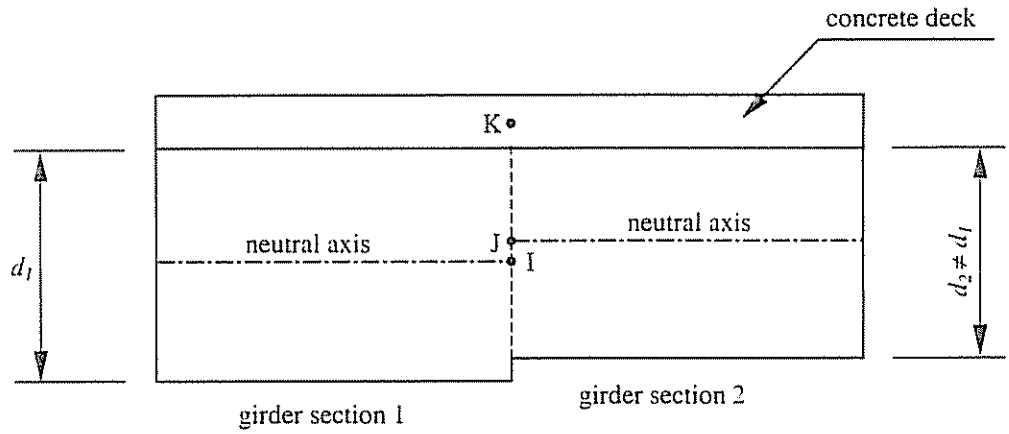

Figure 4.2.5 Modeling of section change

To model this effect constraint equations were again used. Three nodes were created at the interface of a section change, one in the deck and one at the respective centroid of the two girder sections. Then, through constraint equations, the three nodes were rigidly connected as described earlier.

4.2.6 Modeling of Transverse Diaphragm

The transverse diaphragms are cross-frames as shown in Figure 2.5. Although the cross-frames may provide load transfer in six directions, three

translations and three rotations, the main effects were assumed to be in the y and z directions and rotation around x direction. In order to incorporate the effect of the diaphragms in the model, the cross-frames were modeled using equivalent beam elements placed between the girder beam elements.

To determine the sectional properties of the equivalent diaphragm beam element, a model of a typical cross-frame was developed as shown in Figure 4.2.6. Unit loads were applied in each of six directions (translations in the x, y, and z directions, and rotations about the x, y, and z axes) to the rigid body, while deformations in all directions were constrained, except in the direction of the load. The computed deformations were then used to calculate the cross-sectional properties, A_x, I_x, I_y, I_z, of the equivalent beam element used to model the diaphragms.

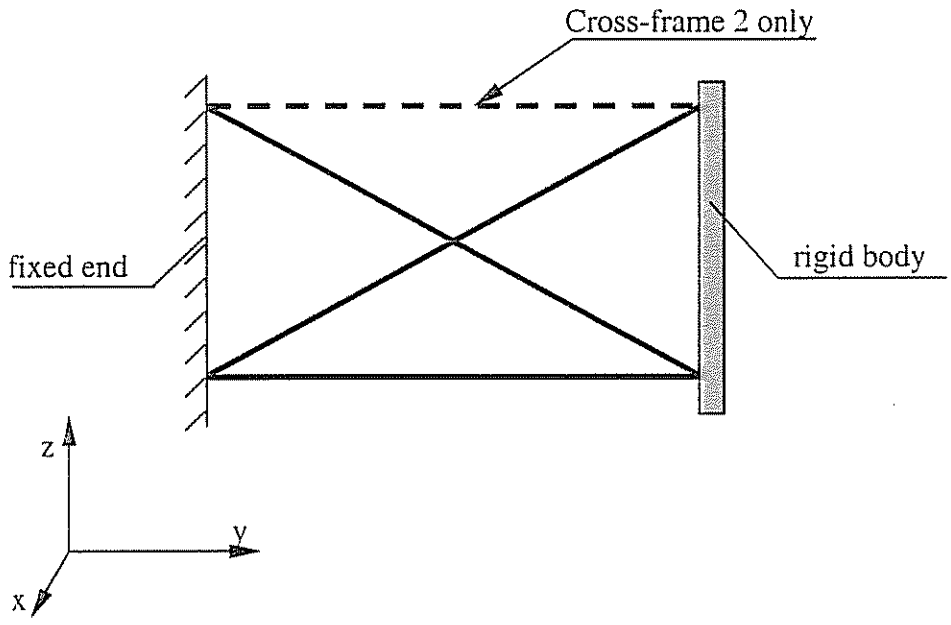

Figure 4.2.6 Model used to determine properties of the diaphragm

4.2.7 Modeling of the Supports

In the analyses, two methods were used to model the supports. The actual bridge girders are supported at the ends on expansion bearings and are continuous over the center pier, supported by fixed bearings. Details of the bearings are shown in Figures 2.6 and 2.7. For the expansion bearing (i.e., at the girder ends), translations in the transverse and vertical directions (y and z directions) are restrained, while longitudinal translation and all rotations are free. For the fixed bearing (i.e., over the center pier), translations in all three directions are restrained while all rotations are free.

In method one, support conditions (i.e., fixities) were imposed directly to the beam element nodes, as shown in Figure 4.2.7(a). At the ends of girders, the translations in the y and z directions were set equal to zero, while the translation in the x direction and all rotations were free. At the intermediate support, the translations in the x, y, and z directions were set equal to zero, while the all rotations were free.

In method two, nodes at the centers of the spherical surfaces of the bearings, (Figures 2.6 and 2.7), were created, as shown in Figure 4.2.7(b). All support conditions, which were the same as in method one, were applied to these newly added nodes. The beam element nodes directly above the bearing were then rigidly connected to these nodes by constraint equations, as outlined in Section 4.2.4. This method allowed for movements of the support to be simulated.

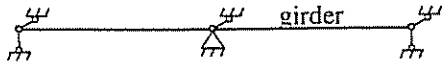

a. Method one

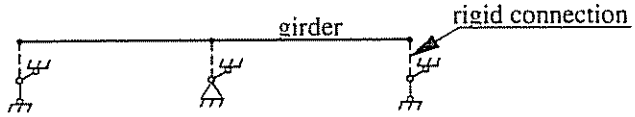

b. Method two

Figure 4.2.7 Modeling of the supports

4.3 Load Cases

Unless otherwise noted, the load case used in the analyses that follow was from pass 11 of the field test with the truck located to cause the peak strain (see Figure 4.3.1). Truck 2851 was straddling the center line and truck 2844 was passing with the driver side wheel was on the left yellow line.

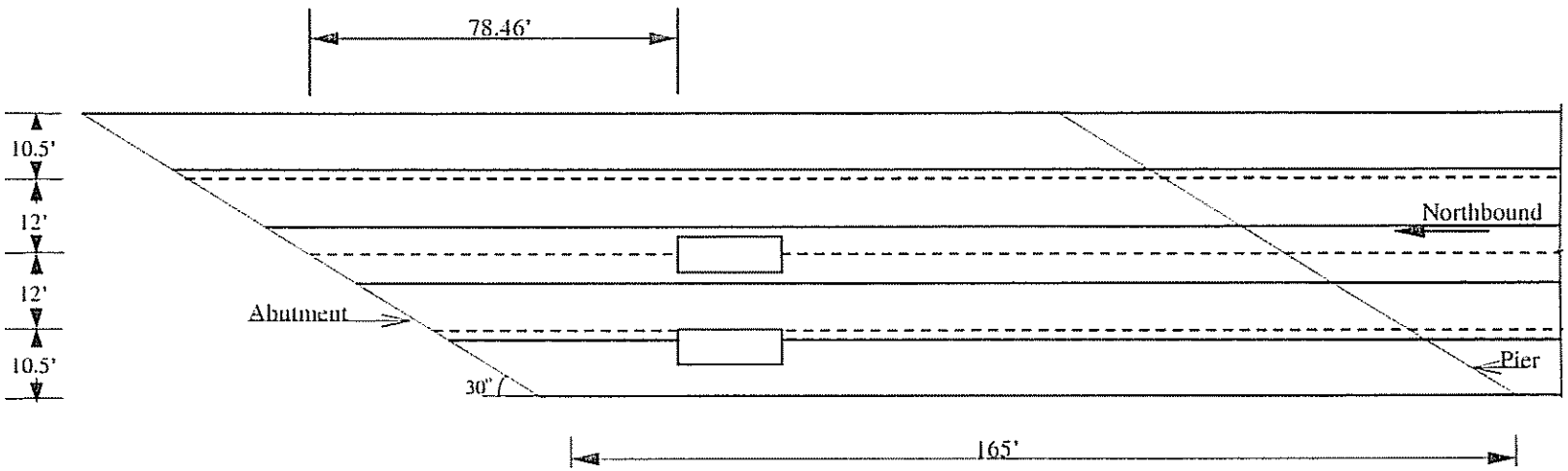

Figure 4.3.1. Load case

4.4 Results

4.4.1 Influence of Mesh

The finite element method is a numerical method that gives approximate results. The accuracy of the calculations depend on the size of the element mesh. It is important that the model mesh be fine; however, it becomes uneconomical to use a model with too fine of a mesh. To determine the necessary mesh size, a convergence study was conducted. The criterion for determining the accuracy of the solution was based on the difference between the results from a given mesh to a more refined mesh.

Two meshes were used in the study. The first one had a distance of five feet between shell element nodes and five feet between beam element nodes (referred to here as the "coarse" model). The second one had a distance of one foot between shell element nodes and one half foot between beam element nodes (referred to here as the "fine" model). Results of the two models are shown in Table 4.4.1 and Figure 4.4.1. Table 4.4.1 presents the strain values calculated at the transducer locations from the field test; Figure 4.4.1 shows the axial strain in the bottom flange of each girder. As the axial strain in the bottom flange is an extremum at every location and the test measurement with which we are going to compare was the axial strain in the bottom flange, we chose it as the criterion in the convergence study.

Note that the difference between the two models is very small, although the second one was a few times finer than the first. The relative difference at most locations is less than five percent, except where the computed strains were very small. Note that the very small computed and measured strains are more susceptible to numerical and experimental error, and therefore, the relative differences tend to be large. Figure 4.4.1 shows that the difference between the two models is very small.

Although the difference is small, the fine model gives better results. Based on these results, all subsequent analyses were conducted using the fine mesh model.

Table 4.4.1 Strains calculated by the fine and coarse models

Transducer number	302	294	308	350	337	300	
coarse model	2.7	16.3	18.0	13.8	0.3	-15.6	
fine model	1.7	15.7	17.4	13.3	-1.3	-18.7	
relative difference (%)	60.2	4.3	3.7	4.0	-121.2	-16.4	
Transducer number	319	297	309	346	316	306	307
coarse model	0.0	-1.3	17.4	27.9	28.6	1.3	-13.7
fine model	0.0	-1.8	16.6	27.0	28.0	0.9	-15.4
relative difference (%)	0.0	-28.4	5.2	3.2	2.3	55.3	-11.5
Transducer number	298	317	314	295	304		
coarse model	-5.8	13.8	54.6	-10.9	-26.8		
fine model	-5.9	12.6	53.0	-12.1	-27.8		
relative difference (%)	-1.2	9.0	3.1	-9.6	-3.7		
Transducer number	318	353	341	296	292	338	312
coarse model	0.9	-5.7	12.3	71.3	75.7	-17.1	-25.8
fine model	0.6	-5.6	8.0	70.2	74.9	-17.9	-26.1
relative difference (%)	57.1	1.6	53.1	1.7	1.0	-4.3	-1.3
Transducer number	351	345	291	305	320		
coarse model	3.7	80.7	52.4	-15.0	-17.9		
fine model	4.1	78.8	51.9	-15.1	-17.7		
relative difference (%)	-8.1	2.4	1.1	-0.9	1.2		
Transducer number	348	344	356	339	315	343	
coarse model	-4.4	67.9	77.9	40.1	-12.4	-16.4	
fine model	-0.9	66.2	75.7	39.0	-11.4	-16.3	
relative difference (%)	410.5	2.7	2.9	2.7	8.0	0.6	

a. Girder 1

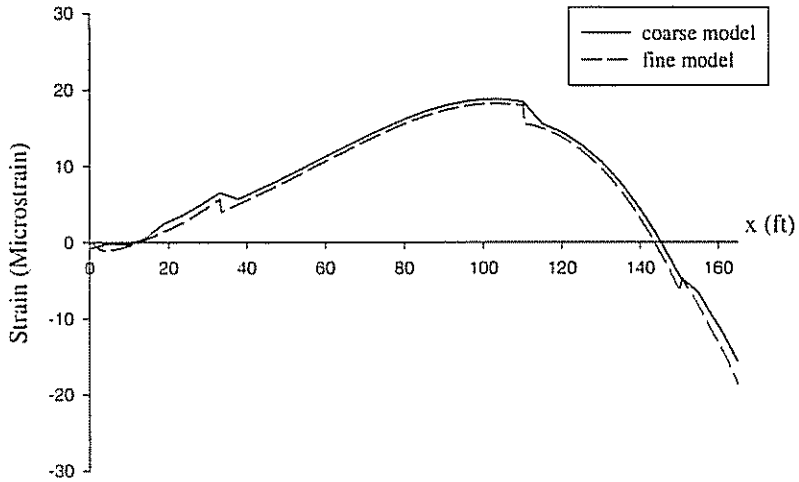

b. Girder 2

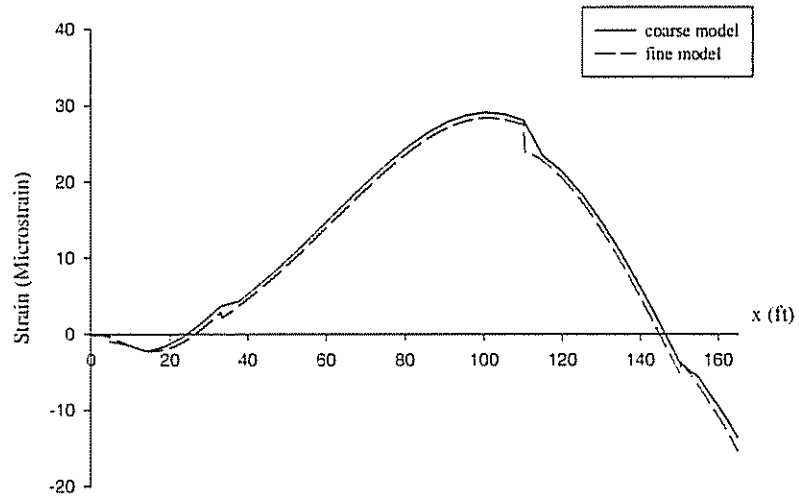

Figure 4.4.1 Strain distribution calculated by the fine and coarse models

c. Girder 3

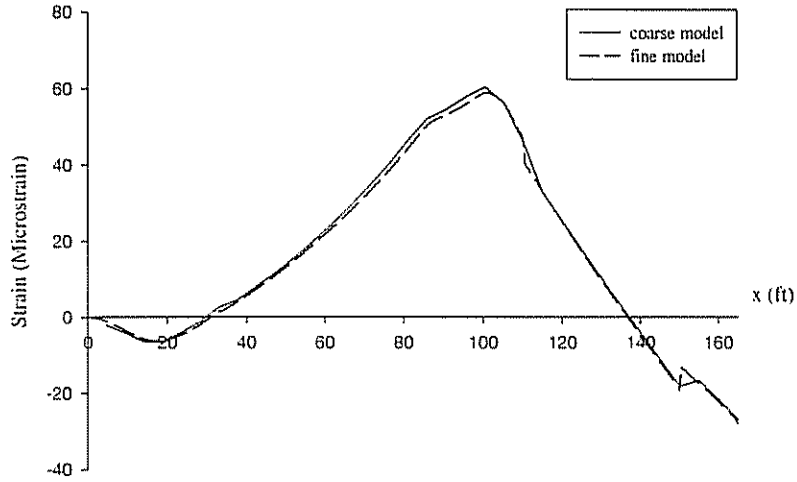

d. Girder 4

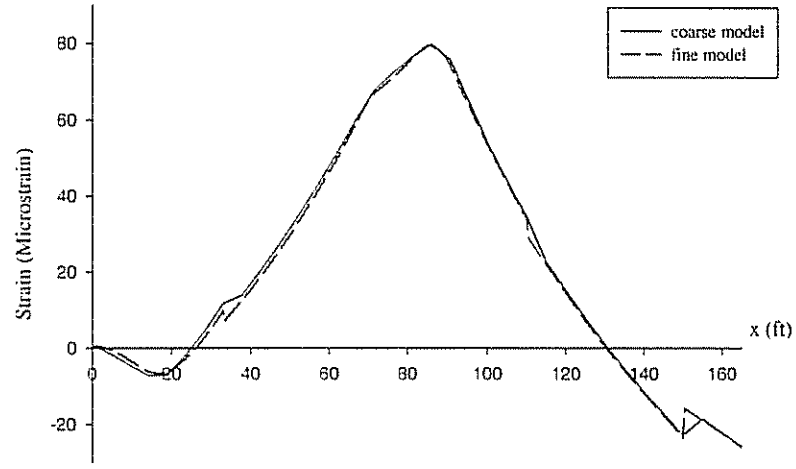

Figure 4.4.1 (continued) Strain distribution calculated by the fine and coarse models

e. Girder 5

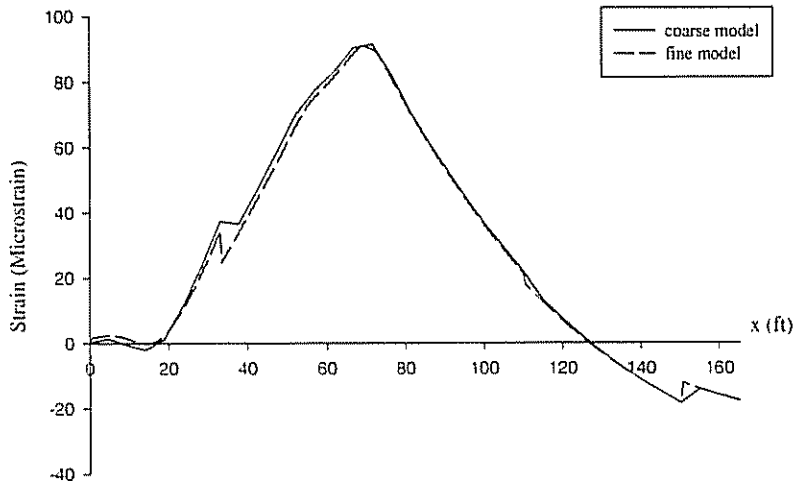

f. Girder 6

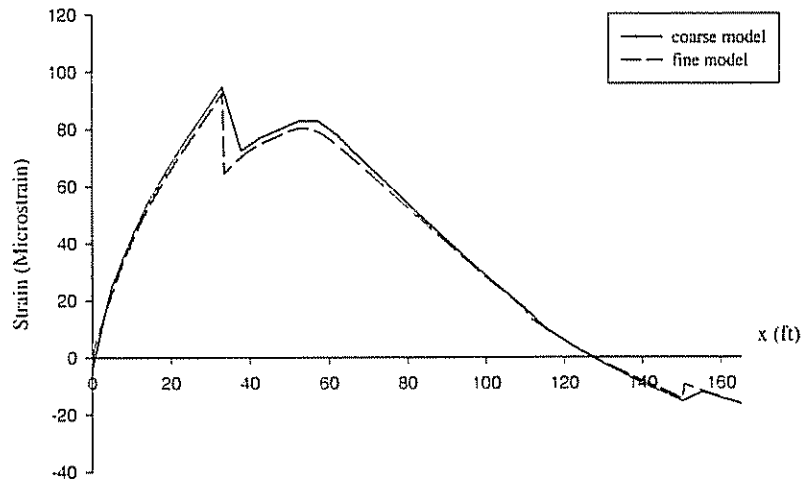

Figure 4.4.1 (continued) Strain distribution calculated by the fine and coarse models

4.4.2 Influence of Transverse Stiffness

The girders were connected by the concrete deck and diaphragms, which transferred truck loads transversely between girders. The stiffness of the deck and diaphragm played a key role in the load distribution. The influences of deck stiffness and diaphragm stiffness were analyzed separately.

4.4.2.1 Influence of the Elastic Modulus of Concrete

The bridge model used to study the effect of concrete modulus did not include transverse diaphragms. The first analysis was based on a nominal elastic modulus for concrete of 3,824 ksi (26.37 KN/mm^2), which was calculated from the concrete strength designated in the construction drawings (f_c'=4.5 ksi). Analyses were then conducted with a modulus 10% greater and a modulus 10% less than the nominal value. Results of the analyses are shown in Figure 4.4.2.

Note that the influence of the elastic modulus of concrete of deck was negligible, i.e., small variations in the elastic modulus about the nominal value had little or no influence on the computed results. The results suggest that for a bridge of this type, slight variations in concrete modulus will have little or no influence on the transverse load distribution in the bridge. The nominal modulus for concrete was used in all subsequent analyses.

a. Girder 1.

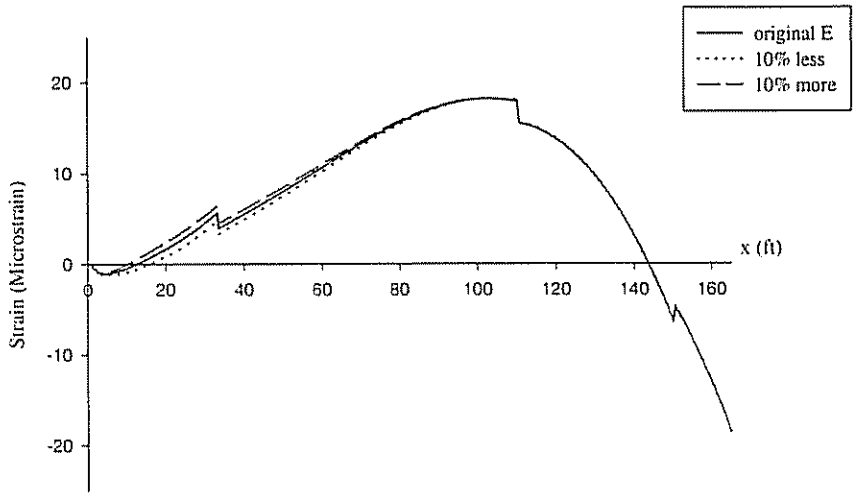

b. Girder 2

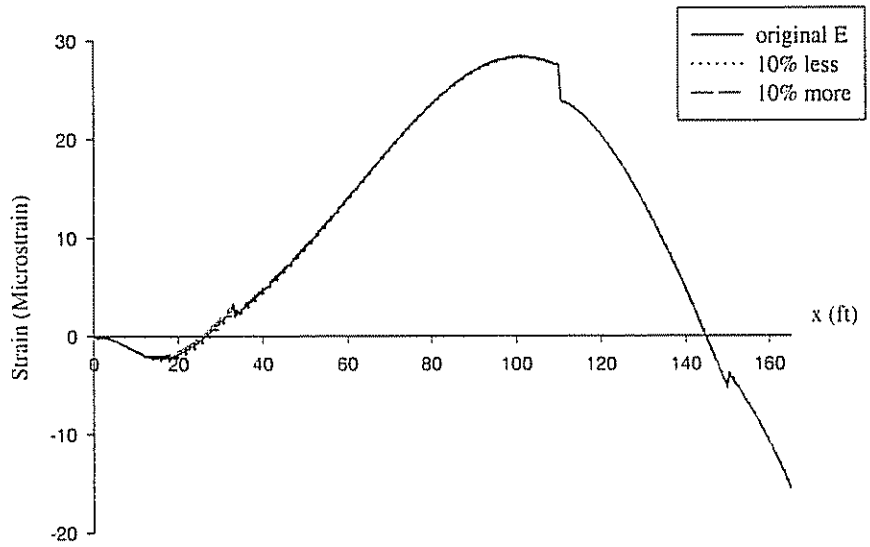

Figure 4.4.2 Effect of the elastic modulus of concrete of the deck

c. Girder 3

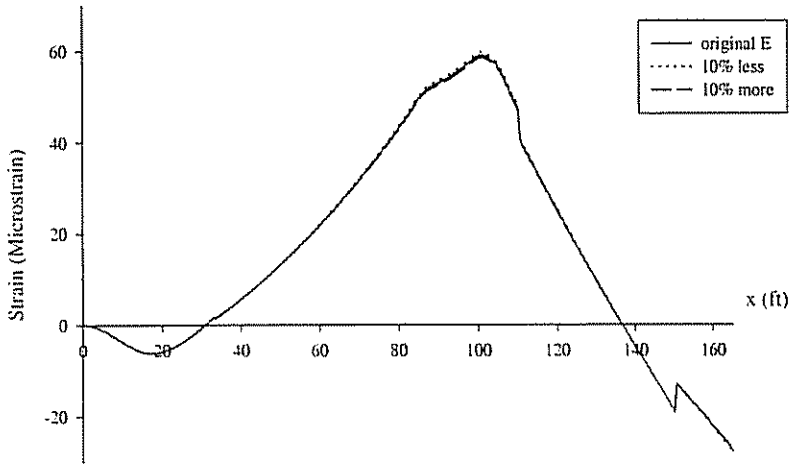

d. Girder 4

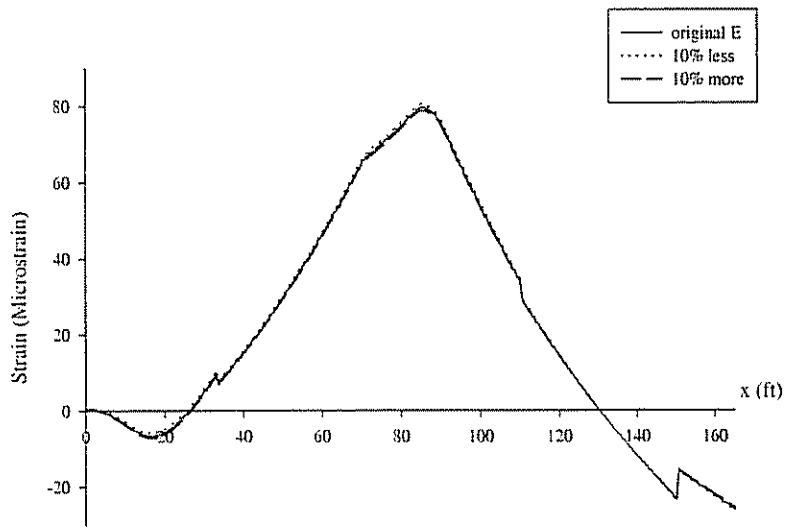

Figure 4.4.2 (continued) Effect of the elastic modulus of concrete of the deck

e. Girder 5

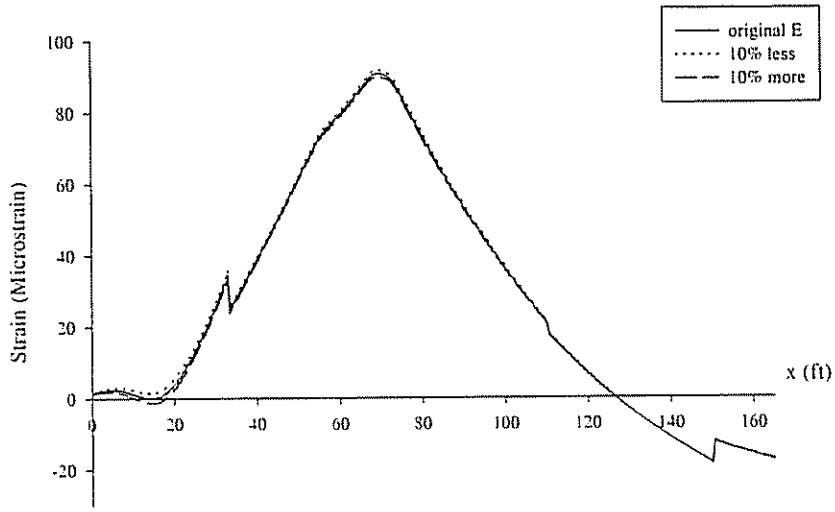

f. Girder 6

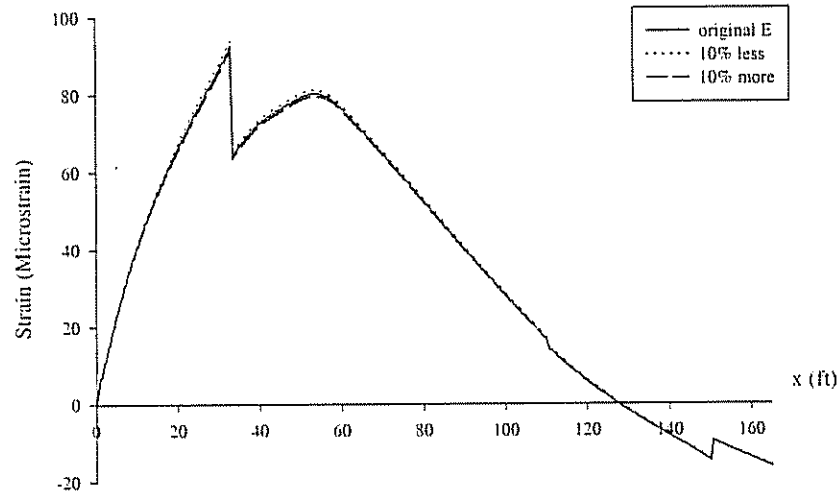

Figure 4.4.2 (continued) Effect of the elastic modulus of concrete of the deck

4.4.2.2 Influence of the transverse diaphragms

In this section, the influence of the transverse diaphragms and diaphragm stiffness were analyzed. Three different cases were considered: diaphragms with the stiffness calculated from the real cross-frames, diaphragms with one half the calculated stiffness and finally, no transverse diaphragms. Results of the analyses are shown in Figure 4.4.3.

Note that the influence of diaphragms is significant. When diaphragms are included the maximum positive strain in the girder away from the load increases (Figure 4.4.3(a)) and the strain in the girder under the load truck decreases (Figure 4.4.3(c)) relative to the case without diaphragms. This suggests that the diaphragms played a role in transverse load distribution. As a result, the capacity of an individual girder needed to carry the live load is somewhat lower than it would be if no diaphragms were used.

Another interesting effect of the diaphragms is revealed at the pinned ends of the girder. Without diaphragms the strain at the support is identically zero. However, for the case with diaphragms at the pinned ends of girders away from the loads (Figure 4.4.3, acute corner), positive strains appeared, and at the pinned ends of girders under the loads (Figure 4.4.3, obtuse corner), negative strains appeared. Due to these negative strains at the pinned ends, positive strains at the middle of the span are reduced.

Results show that the strains in the girders away from the load became lower and the strains in the girders under the load became larger when the stiffness of the diaphragms are reduced. Note, however, comparing the case with the full stiffness to the case with one half the stiffness, the difference in the peak strains is not significant. Also, it seems that the influence of diaphragm is not linear.

The only factor to explicitly account for transverse stiffness of the bridge in the AASHTO load distribution equations ((1.1) and (1.2)) is t_s, the thickness of the deck. As discussed above, diaphragms appear to play some role in the load distribution of a skewed bridge. More research and testing needs to be done to investigate the influence of diaphragms on the load distribution in skewed bridges and, if necessary, to account for their presence in the code load distribution equations.

4.4.3 Influence of Supports

In this section, two methods of support modeling are presented. In the first model, the support conditions were imposed directly to the beam element nodes. In the second, nodes at the center of the spherical surfaces of the bridge bearings were created and the support conditions were imposed to these nodes. The end nodes of the beam elements were connected rigidly to the bearing nodes through constraint equations. The second modeling method was considered to be much closer to the actual support conditions. Results of the two analyses are shown in Figure 4.4.4.

Note that the difference between the two modeling methods was insignificant. Although the second approach more accurately represents the true constraints provided by the bridge bearings, the first approach was found to be adequate and had little influence on the overall computed response.

a. Girder 1

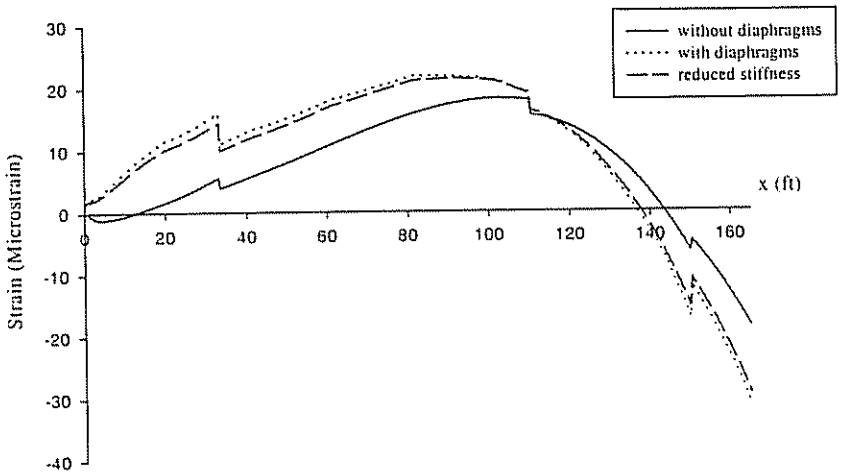

b. Girder 2

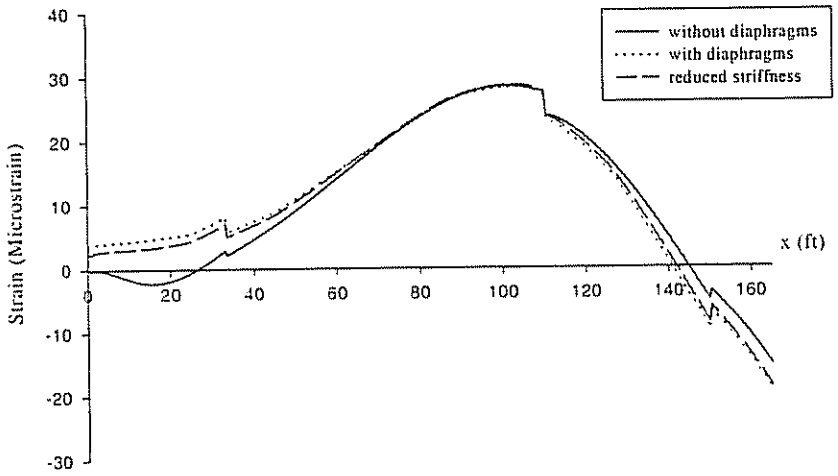

Figure 4.4.3 Effect of diaphragms

c. Girder 3

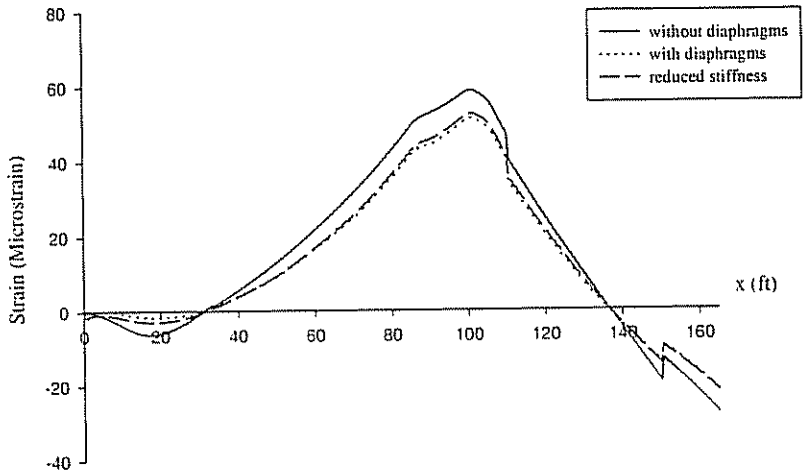

d. Girder 4

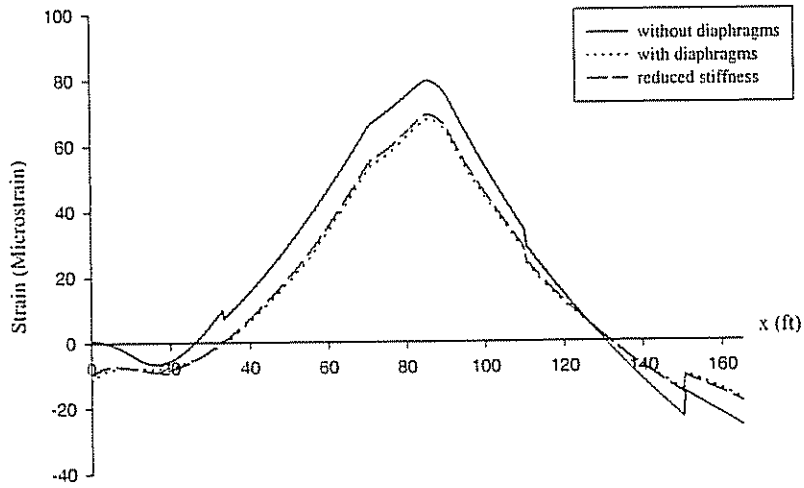

Figure 4.4.3 (continued) Effect of diaphragms

e. Girder 5

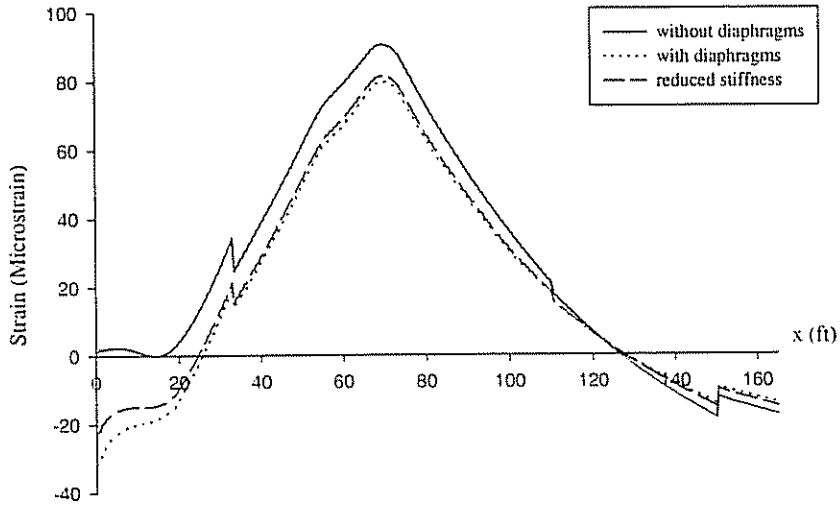

f. Girder 6

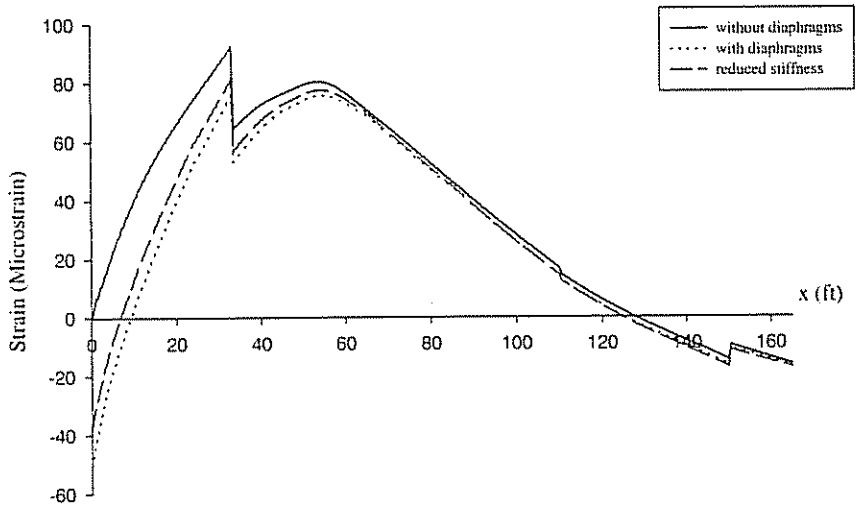

Figure 4.4.3 (continued) Effect of diaphragms

a. Girder 1

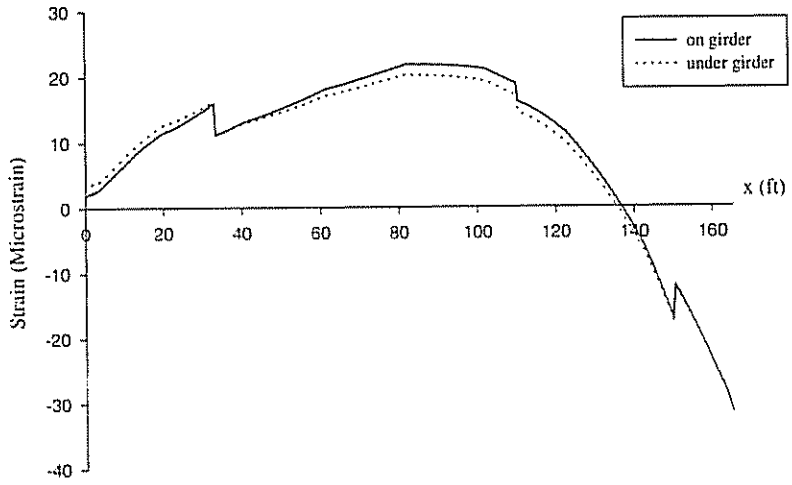

b. Girder 2

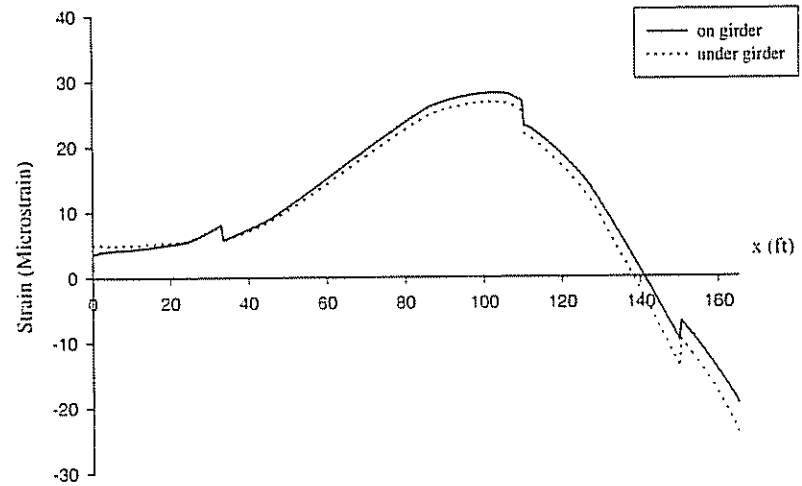

Figure 4.4.4 Influence of support modeling

c. Girder 3

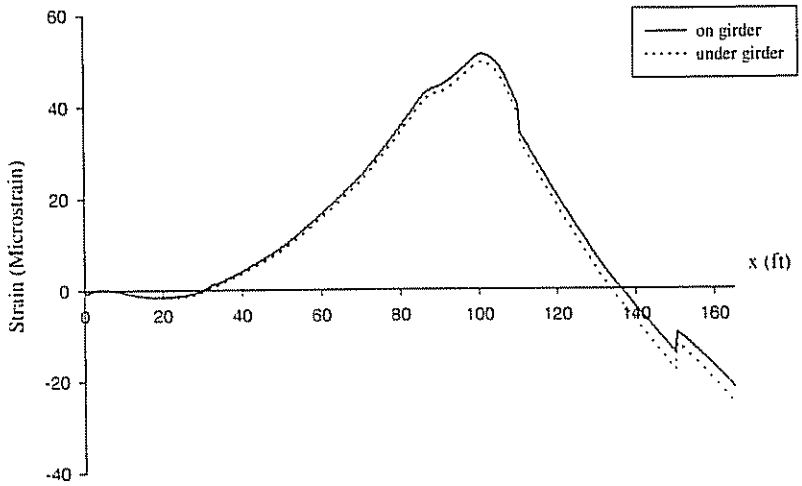

d. Girder 4

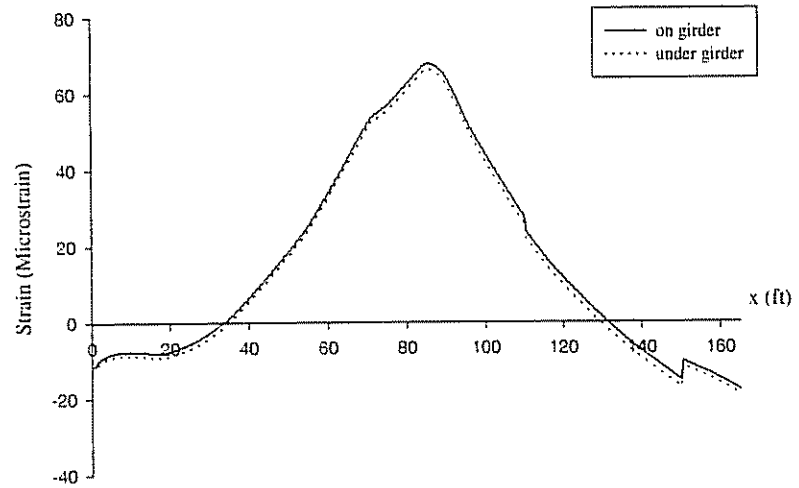

Figure 4.4.4 (continued) Influence of support modeling

e. Girder 5

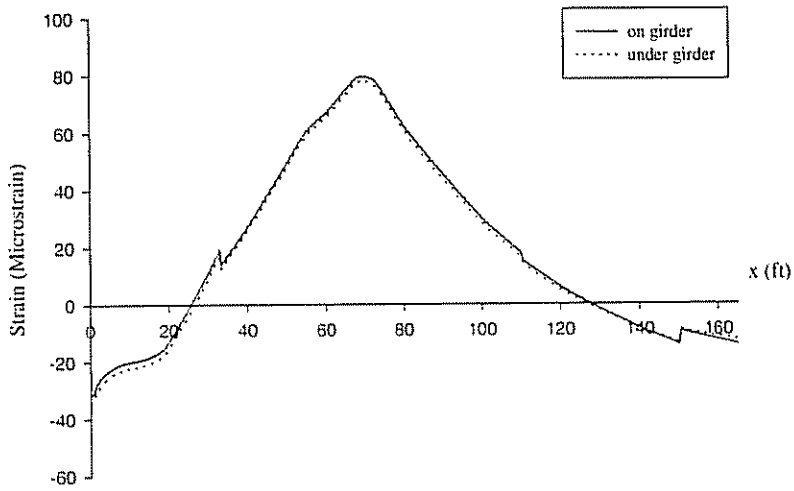

f. Girder 6

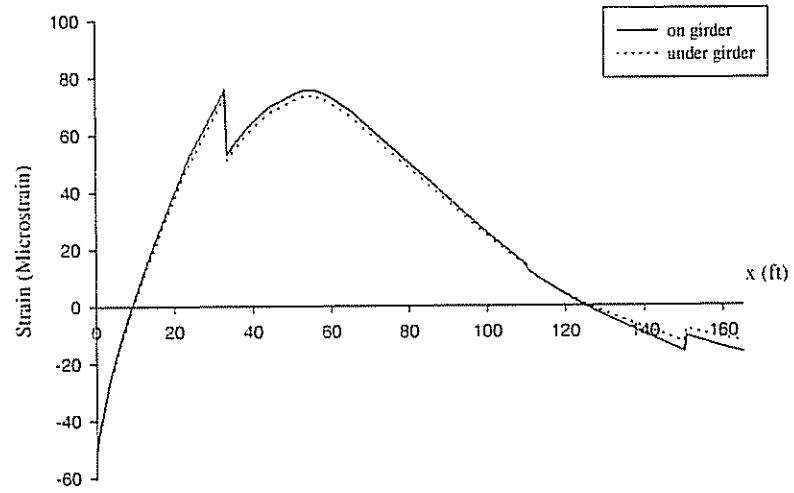

Figure 4.4.4 (continued) Influence of support modeling

4.4.4 Comparison with Test Results

In this section the analytical results are compared with the field test results. Strains in the bottom flange along the girders are compared in detail for two load cases, pass 11, which corresponded to one truck straddling the center line and one truck with the passenger side wheel on the left line, and pass 12, which corresponded to one truck straddling the center line and one truck with the driver side wheel on the right line (Figure 3.3.1). These load cases were selected for detailed comparison because they caused the largest strains measured during the test. The computed and measured peak strains at all gage locations are then compared for all 13 truck passes.

The model used here had the sectional properties of the actual steel girders (Table 4.2.1), diaphragms with the stiffness calculated from the actual cross-frames as described in Section 4.2.6, the elastic modulus of concrete of $E = 3{,}824$ ksi calculated from the concrete strength designated in the construction drawings ($f_c^{'} = 4500\,\text{psi}$) and the support conditions imposed directly to the end nodes of the girders. Presented in Figure 4.4.5 are the results for pass 11 and in Figure 4.4.6 are the results for pass 12. All the results are with the truck in the location that caused the maximum positive strain to occur.

a. Girder 1

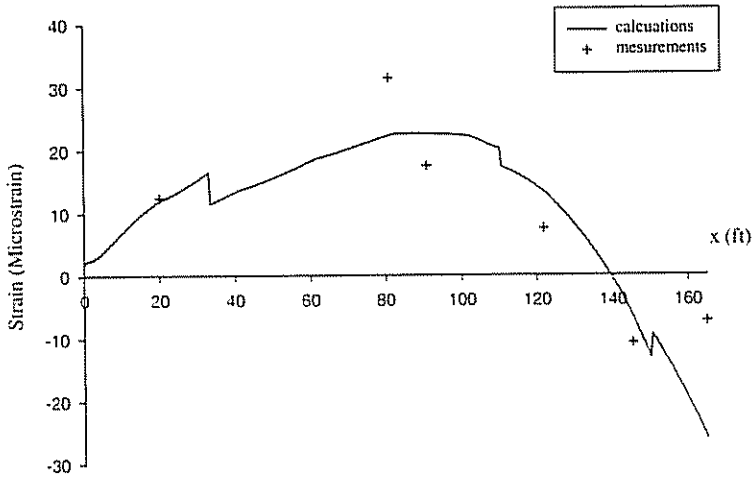

b. Girder 2

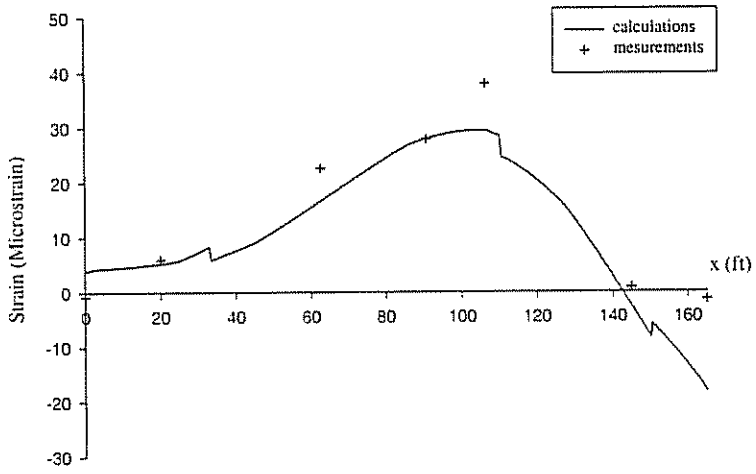

Figure 4.4.5 Measurements and calculations for pass 11

c. Girder 3

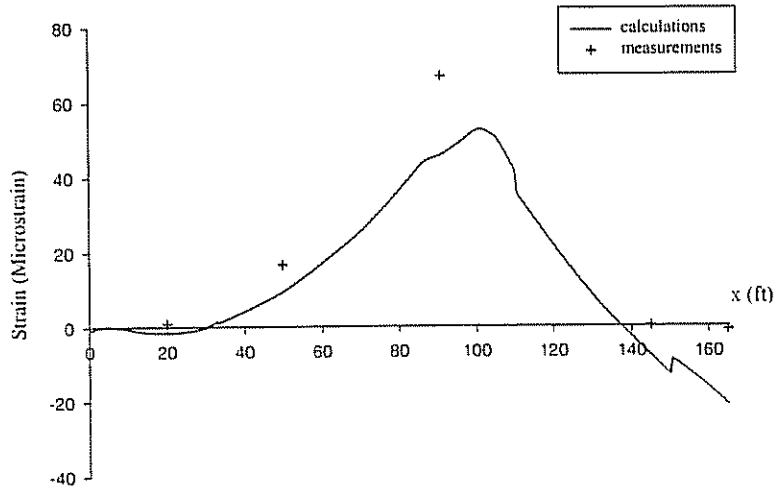

d. Girder 4

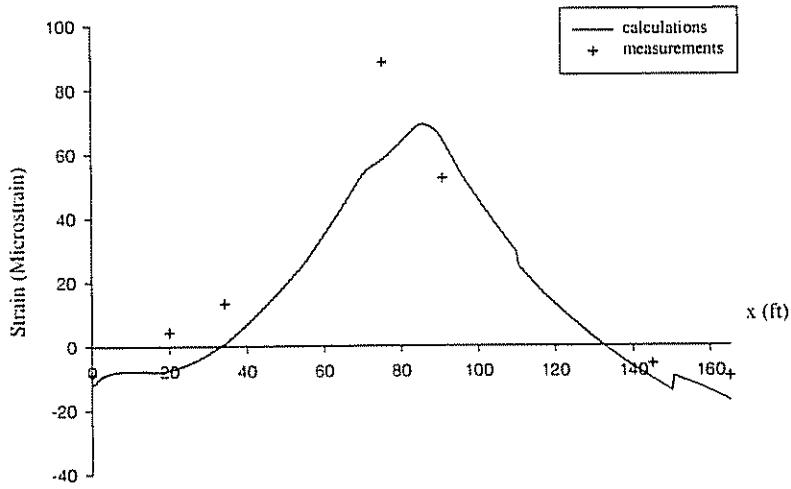

Figure 4.4.5 (continued) Measurements and calculations for pass 11

e. Girder 5

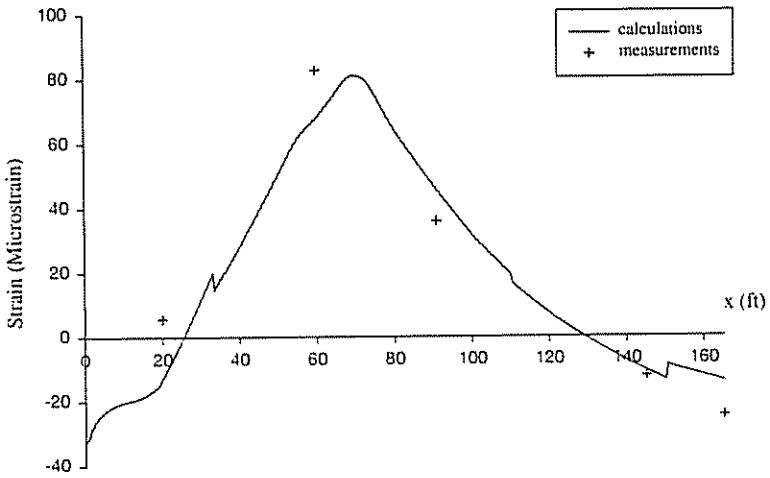

f. Girder 6

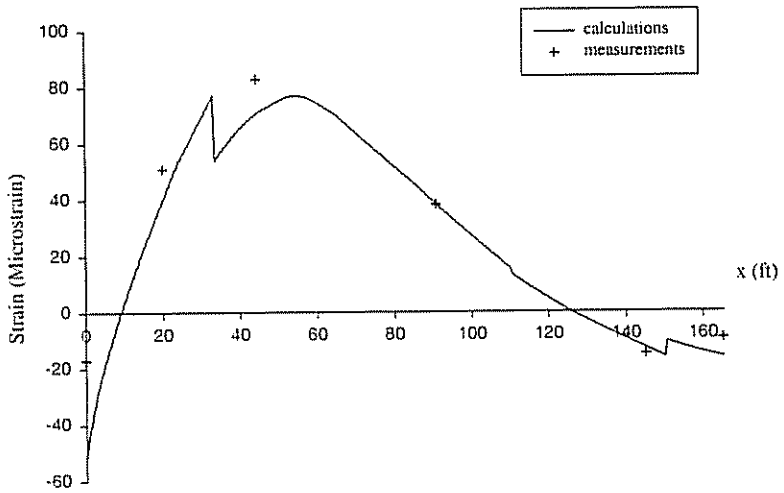

Figure 4.4.5 (continued) Measurements and calculations for pass 11

a. Girder 1

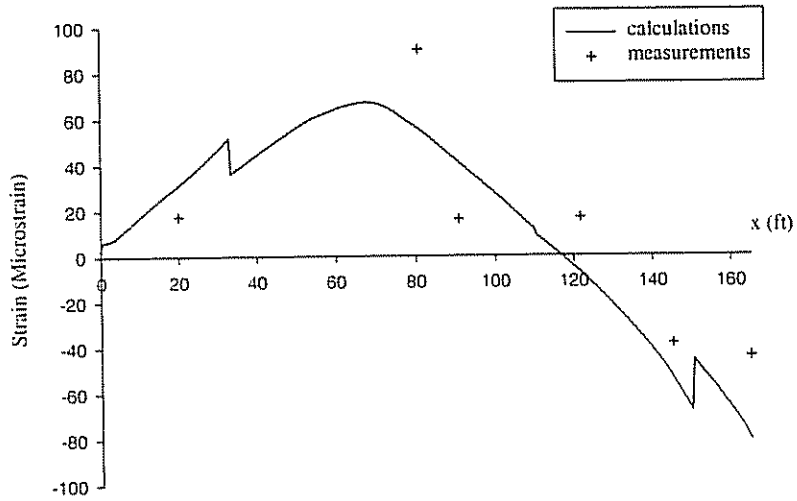

b. Girder 2

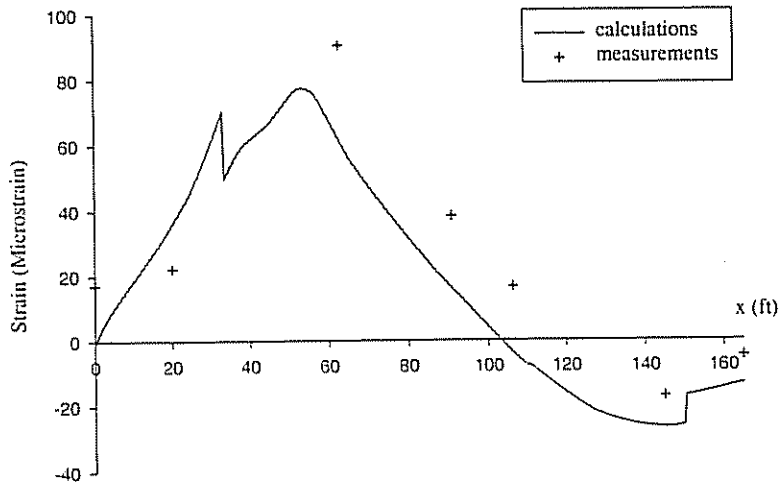

Figure 4.4.6 Measurements and calculations for pass 12

c. Girder 3

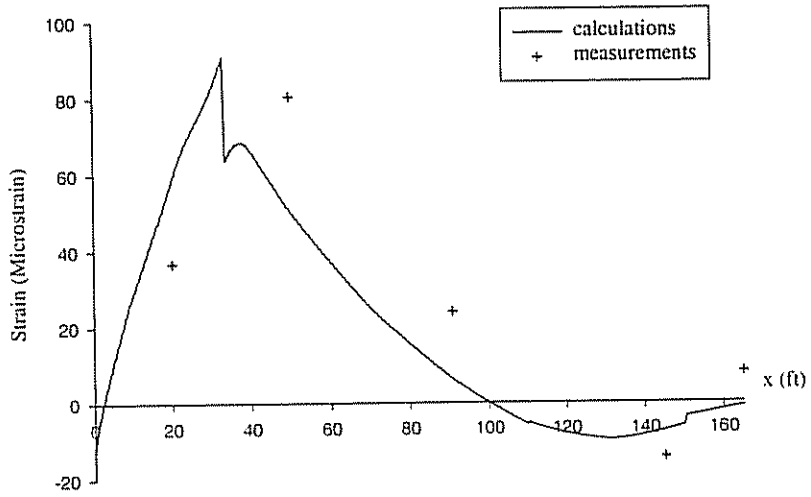

d. Girder 4

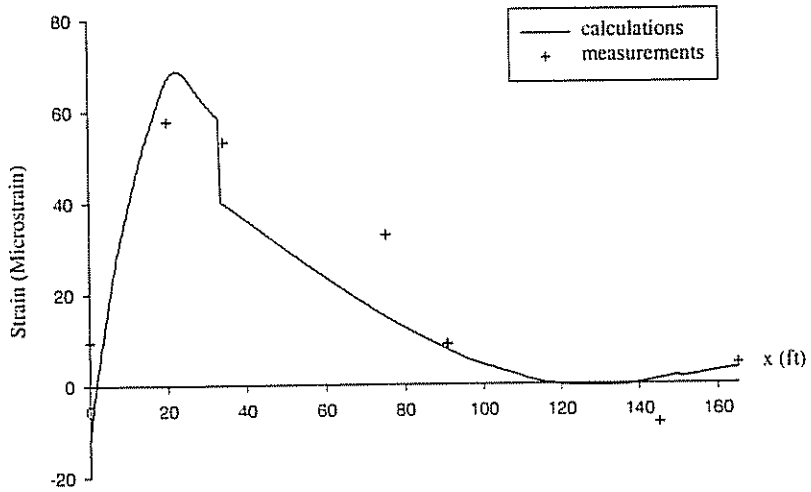

Figure 4.4.6 (continued) Measurements and calculations for pass 12

e. Girder 5

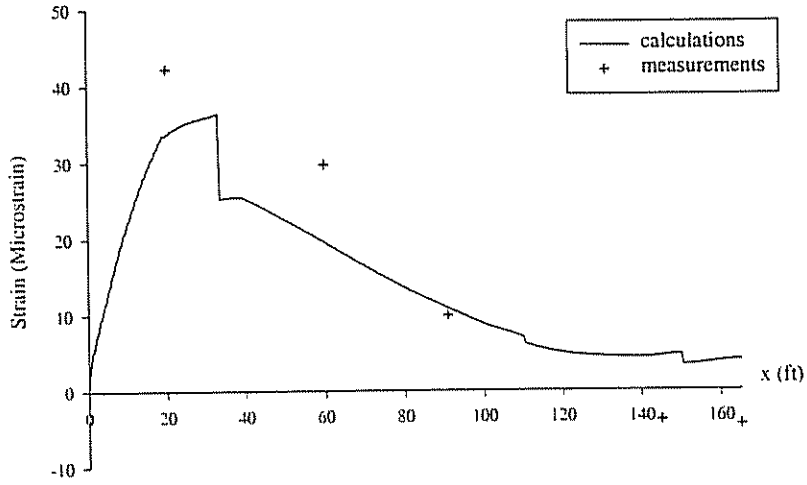

f. Girder 6

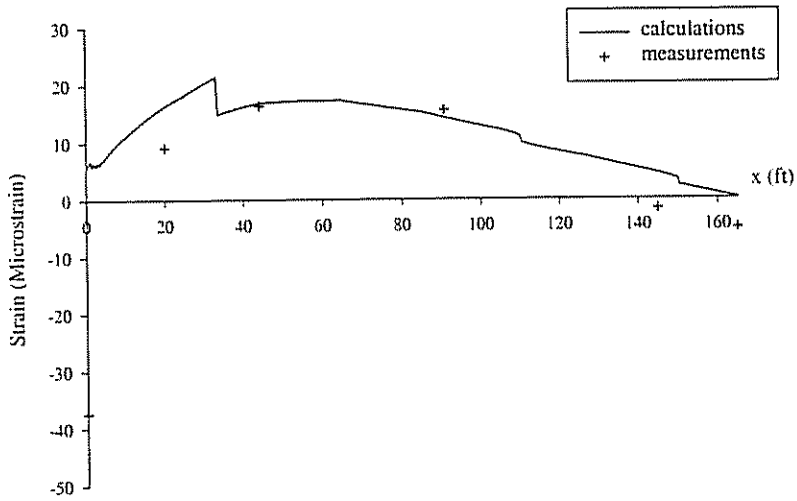

Figure 4.4.6 (continued) Measurements and calculations for pass 12

Note that the analytical results are in good agreement with the measured data, particularly in the left side of the bridge (girder 5 and 6) for both passes 11 and 12. It is evident that the numerical model is slightly stiffer than the real structure, i.e., the model predicts smaller strains than recorded in the girders farthest from the load. The computed strains had the same shapes as the measured strains. For pass 11, the difference between the analytical results and the measured strains in the girders away from the loads, i.e., on the right side of the bridge, were slightly larger than that at the girders under the loads, i.e., the left side of the bridge. For pass 12, in which one truck moved to the right side of the bridge, the difference between the calculations and the measured strains in the girders away from the loads were a little smaller than those in the girders under the loads. Similar to the pass 11 calculations, the measurements are closer at the left side of the bridge than at the right side. The strains calculated along girder 6 were very close to the measurements. It was observed that the strains calculated at the supports were larger than the measured strains. Overall, the analytical model was stiffer than the real structure, although the results are generally consistent with the measurements.

One possible explanation for the model being stiffer is that in the negative moment region the concrete is in tension, which would yield a lower effective stiffness of the composite section than used in the model. As shown in Figure 4.4.5(f), the calculated strain at the pinned end of girder 6 is 51 με in tension, while the measured strain at the same location is 17 με in tension. This localized stiffer may also be a reason for the model being stiffer than the actual strucuture.

Presented in Table 4.4.2 are the measured and calculated peak strain for all 13 truck passes. The calculated values were obtained with the truck(s) in the position

on the bridge that caused the maximum strain. Also shown is the percent difference in the calculated and measured values. The differences range from a low of 1% for pass 12 to a high of 27% for pass 5. The calculated values are consistently smaller than the measured values which again indicates that the model is stiffer than the actual bridge.

Table 4.4.2 Measured and calculated peak strain for each pass due to the truck(s) being at the location that caused the peak strains

Pass	measured ε^{+}_{max} (με)	calculated ε^{+}_{max} (με)	δ (%)
1	72	56	-22.2
2	65	58	-10.8
3	49	45	-8.2
4	51	46	-9.8
5	52	38	-26.9
6	57	42	-26.3
7	54	45	-16.7
8	56	49	-12.5
9	59	54	-8.5
10	92	78	-15.2
11	91	81	-11.0
12	90	91	1.1
13	94	82	-12.8

measured ε^{+}_{max} is the maximum positive strain measured.

calculated ε^{+}_{max} is the maximum positive strain calculated at the location of the measured maximum strain.

δ is the relative difference =(calculated-measured)/measured

4.4.5 Comparison with AASHTO code

The AASHTO code provides a load distribution factor method to determine the maximum moments in the interior and exterior girders for designing and evaluating a bridge. The equations for the distribution factor were presented earlier in Chapter 1. One girder with the same support conditions was loaded by one entire truck to determine the maximum positive and negative moments for this single girder. Load distribution factors at the locations of maximum strains for interior and exterior girders were calculated using the AASHTO formulas considering the effect of skew. Then these factors were applied to the maximum moments calculated in the single beam to obtain the design moments for the girders. Based on the moments, maximum positive and negative strains were calculated and compared with the test results. The results are presented in Table 4.4.3.

Table 4.4.3 Maximum positive and negative strains in girders

	positive strains (με)		negative strains (με)	
	interior	exterior	interior	exterior
AASHTO code	131	101	46	47
Test	94	89	45	48
Model	91	77	27	70

It can be seen that the AASHTO formulas over-predict the maximum positive strains in girders, which is quite common in a right bridge. The AASHTO formulas very accurately predict the maximum negative strains in girders, which shows that the skew effect has different influences on positive or negative moments. The AASHTO specifications provided one load distribution factor regardless of

whether the bridge is a single simple span or numerous continuous span. In the test, the load trucks were different from the standard load trucks specified in the AASHTO code. Most previous works were done based on the AASHTO standard trucks. There is little information on the influence of truck types. The calculations are smaller than the results from AASHTO code. Mabsout, et al. (1997) pointed out that load distribution factors obtained for normal bridges using finite element analyses tend to be smaller than those given by AASHTO formulas.

In the AASHTO code, the only factor considered for transverse stiffness in determining load distribution factors was the thickness of the deck. The effect of diaphragms was not considered. This may be one reason why test measurements and finite element results are smaller than the AASHTO code. Although higher bending strains result when diaphragms are ignored, it should be noted that the moments at pinned ends will be zero, which may not be the case in the real structure.

Chapter 5

CONCLUSIONS

In this research, a two-span, continuous, slab-on-girder highway bridge with a skew angle of 60° was field-tested. A finite element method was used to analyze the bridge. The influence of mesh size, elastic modulus of the deck concrete, diaphragms, and support modeling were studied. The results were compared with the AASHTO LRFD specifications.

For one load truck, the maximum measured positive strain was 72 με and the maximum measured negative strain was 38 με. For two load trucks, the maximum measured positive strain was 94 με and the maximum measured negative strain was 48 με. The maximum positive strains always occurred in the edge girder or one girder in from the edge (i.e., girder 2 or 5). The transverse distribution of strains was parallel to the skew line. Negative moments appeared at the pinned ends at the obtuse corners. The bridge is behaving linearly.

The finite element analyses provided close results to the measured values, although the finite element model was a little stiffer than the real structure. The influence of the slight variation of the elastic modulus of the deck concrete was very small, so it was not a concern in evaluating load distribution of the bridge. Diaphragms played a more important role in the load distribution. After adding diaphragms, load distribution factors decreased. At the obtuse corner of the skewed bridge, negative moments appeared at the pinned ends due to the effect of the diaphragms. It played the same effect of the deck. As shown in the AASHTO load

distribution factor formulas, the stiffness of the deck also influenced the load distribution factors nonlinearly (note the t_s term). As a result, the effect of diaphragms might be considered as an equivalent deck thickness, which would not change the current formulas. It should be noted by designers that the moments at pinned ends of girders may not be zero. In modeling a bridge, support conditions could be applied directly to the end nodes of the girders. The actual geometry and configuration of the bearings did not seem to be a significant factor in the analytical results.

The AASHTO load distribution factor formulas over-predict positive moment and accurately predict negative moments comparing to the measured values. As the AASHTO formulas over-predict in general, the skew effect might have a different influence on positive and negative moments.

REFERENCES

1 American Association of State Highway and Transportation Officials (AASHTO). (1994). *LRFD Bridge design Specifications.*

2 Khaleel, M. A., and Itani, R. Y. (1990). "Live-Load Moments for Continuous Skew Bridges." *Journal of Structural Engineering*, Vol. 116, No. 9, 2361-2373.

3 Zokaie, T., Osterkamp, T. A., and Imbsen, R. A. (1991). "Distribution of Wheel Loads on Highway Bridges." (NCHRP project 12-26), Imbsen & Associates, Inc.

4 Ebeido, T., and Kennedy, J. B. (1996). "Girder Moments in Continuous Skew Composite Bridges." *Journal of Bridge Engineering*, Vol. 1, NO. 1, 37-45.

5 Ebeido, T., and Kennedy, J. B. (1996). "Shear and Reaction Distributions in Continuous Skew Composite Bridges." *Journal of Bridge Engineering*, Vol. 1, No. 4, 155-165.

6 Mabsout, M. E., Tarhini, K. M., Frederick, D. R., and Tayar, C., (1997). "Finite-Element Analysis of Steel Girder Highway Bridges." *Journal of Bridge Engineering*, Vol. 2, No. 3, 84-87.

7 Swanson Analysis Systems, Inc. (1992). "ANSYS User's Manual for Revision 5.0." Houston, TA.

8 American Iron and Steel Institute. (1997). "Four LRFD Design Examples of steel Highway Bridge."

9 Tonias, D. E. (1995). "Bridge Engineering." McGraw-Hill, Inc.

10 Edberg, W. M. (1994). "State-of-the-art Survey in Experimental Load Rating of Bridges."